# Catalytic Activity Of Cu/η-$Al_2O_3$ Catalysts Prepared From Aluminum Scraps In The $NH_3$-SCO and in the $NH_3$-SCR of NO

**Nawel Jraba** ( naweljraba@hotmail.fr )
University of Sfax Faculty of sciences of Sfax
**Thabet Makhlouf**
University of Sfax: Universite de Sfax
**Gerard Delahay**
University of Montpellier: Universite de Montpellier
**Hassib Tounsi**
University of Sfax: Universite de Sfax

**Research Article**

**Keywords:** Cu/η-Al2O3, NH3-SCR, NH3-SCO, H2-TPR, TEM

**Posted Date:** June 14th, 2021

**DOI:** https://doi.org/10.21203/rs.3.rs-550091/v1

# Abstract

Copper loaded η-alumina catalysts with different copper contents have been prepared by impregnation/evaporation method. The catalysts were characterized by XRD, FTIR, BET, UV−vis, $H_2$-TPR and evaluated in the selective catalytic reduction of NO by $NH_3$ and in the selective catalytic oxidation of $NH_3$. The characterization techniques showed that the impregnation/evaporation method permits to obtain highly dispersed copper oxide species on the η-alumina surface when low amount of copper is used (1wt. % and 2 wt.%). The wet impregnation method made it possible to reach a well dispersion of the copper species on the surface of the alumina for the low copper contents Cu(1)-$Al_2O_3$ and Cu(2)-$Al_2O_3$. The latter justifies the similar behavior of Cu(1)-$Al_2O_3$) and Cu(2)-$Al_2O_3$ in the selective catalytic oxidation of $NH_3$ where these catalysts exhibit a conversion of $NH_3$ to $N_2$ of the order of 100% at T > 500°C.

# Introduction

The selective catalytic reduction (SCR) of NO by ammonia in the presence of excess oxygen is considered a mature technology for the removal of NO from stationary sources (Forzatti, 2001; Usberti et al. 2015). Moreover, this technology has been adapted for the modern diesel exhaust after treatment system using urea as the ammonia precursor (urea-SCR) (Goldbach et al., 2017; Jung et al., 2017; Kröcher, 2018; Nova and Tronkoni, 2014; Piumetti et al., 2015; Yuan et al., 2015). This system contains besides the urea delivery device, a catalyst for the selective catalytic reduction of NO with $NH_3$ ($NH_3$-SCR) combined with an ammonia slip catalyst (ASC) for the selective catalytic oxidation of ammonia ($NH_3$-SCO) (Piumetti et al., 2015; Walker, 2016).

Vanadium-based catalysts (V-catalysts) $V_2O_5$-$WO_3$/$TiO_2$ or $V_2O_5$ – $MoO_3$/$TiO_2$ are widely employed in stationary applications since the 1970s (Lai and Wachs, 2018). However, the major drawbacks bounded to the toxicity of vanadium and its weaker activity at low temperature limit the utilization of V-catalysts in automotive applications. Besides, some country regulations such as USA forbid the use of V-catalysts for automotive applications. Therefore, Cu/Fe-exchanged zeolites have been reported as alternative to vanadium-based catalysts because they are active and $N_2$ selective for the $NH_3$-SCR (Boron et al., 2019; Villamaina et al., 2019; Xin et al., 2018) and for the $NH_3$-SCO (Jablonska, 2020). Among all the zeolite-catalysts, Cu/Fe-ZSM-5 and Fe/Cu-BEA are the most extensively investigated in the past 30 years (Hamoud et al., 2019; Villamaina et al., 2019; Xin et al., 2018). Copper-based zeolites are usually more active in the low-temperature (< 350°C) range while iron-based zeolites are more active at higher temperatures (> 350°C). Small-pore zeolite Cu-SSZ-13 has received great attention due to its higher activity and selectivity at low temperatures and improved hydrothermal stability for diesel vehicles. (Gao and Szanyi, 2018; Lambert, 2019; Shibata et al., 2019)

On the other hand, noble metals (Pt, Pd, and Rh) supported on metal oxides have been studied for the diesel exhaust after treatment system. Common metal oxides such as $Al_2O_3$, $SiO_2$, $CeO_2$, $TiO_2$, and $ZrO_2$

are used as support materials for the diesel oxidation catalyst (Jablonska, 2015; Sun et al., 2019). Nevertheless, γ-$Al_2O_3$ due to its high surface area (100–200 $m^2$/g) and its good thermal stability is preferred to all other metal oxides (Kong et al., 2020; Panahi and Delahaye, 2017). For instance, Pt-γ-$Al_2O_3$ is used in the diesel oxidation catalyst (DOC) and ammonia slip catalyst (ASC) (svintsitskiy et al., 2020). The DOC oxidizes CO, unburnt hydrocarbons and NO in the exhaust gas to $CO_2$, $H_2O$ and $NO_2$, respectively. The ASC removed the excess of $NH_3$ by selective catalytic oxidation (SCO) with oxygen to $N_2$ and $H_2O$. Pt-γ-$Al_2O_3$ catalyst is considered to be the most active for ammonia oxidation below 300°C than the other noble metals (Pd, and Rh).However,Pt-γ-$Al_2O_3$ catalyst has high selectivity towards $N_2O$ and NO over 300°C (Hansen et al.,2017). The drawbacks of noble-metal catalysts motivate the vehicle manufacturers to reduce their content or substitute them with cheaper Mn/Cu-based oxides catalysts (Damma et al., 2019). Indeed, CuO/γ-$Al_2O_3$ catalyst has been proposed to substitute the noble metal-based emission control catalysts in the $NH_3$-SCR (Jeong et al., 1999; Kwak et al., 2012; Xie et al., 2004) and $NH_3$-SCO (Ghosh et al., 2020; Jablonska et al., 2018; Jablonska, 2015; Strom et al., 2018). Major challenges are associated with the design of a suitable downstream catalyst: (i) the catalyst should exhibit high activity at relatively low temperatures (< 400 ∘C) in order to avoid the need for additional heating of exhaust gases, (ii) the material has to possess sufficient stability in the presence of high concentrations of water vapour or other components of waste gases (COx, SOx) and (iii) should selectively convert NH3 into N2 (Jablonska et al., 2016). In NH3-SCO, almost 100% conversion of ammonia is required in order to eliminate ammonia odour. Altogether, a design of oxidation catalysts of high efficiency, selectivity to N2 and stability remains challenging. A promising class of catalysts are Cu based systems which will be discussed more comprehensively in the following (Jablonska and Regina, 2016). In the order of Il’chenko and Ivanovna (1976), copper oxide was found as one of the most efficient catalysts in selective ammonia oxidation into nitrogen and water vapour. Further studies over preoxidised polycrystalline copper foil proved copper oxide as active phase for $NH_3$-SCO. However, due to unsatisfying selectivity to $N_2$, further studies concerning ammonia oxidation over copper oxide supported e.g. on -$Al_2O_3$ (Strom et al., 2018) were carried out.

In our previous work (Jraba et al., 2018), we reported the preparation of γ-$Al_2O_3$ and η-$Al_2O_3$ with high surface areas using aluminum chips collected from metal manufacturing industry as starting materials. η-$Al_2O_3$ and γ-$Al_2O_3$ were obtained by calcination at 500°C of bayerite (α-$Al(OH)_3$) and pseudo-boehmite, respectively. γ-$Al_2O_3$ and η-$Al_2O_3$ are considered to be the most important among other alumina’s due to their high specific surface area (200–500 $m^2$/g) and acid-base properties. Particularly, γ-$Al_2O_3$ counts for the most important industrial applications as adsorbents, catalysts and catalyst supports. To our best knowledge, η-$Al_2O_3$ has never been employed as support for the preparation of CuO/ $Al_2O_3$ catalysts for the $NH_3$-SCR of NO and for the $NH_3$-SCO. Thus, this work is devoted to the preparation, characterization and catalytic activity of copper loaded η-alumina catalysts in the reactions, in presence of water vapour, of $NH_3$ –SCR of NO and of $NH_3$-SCO. The prepared catalysts were characterized by XRD, SEM, TEM, $NH_3$-TPD, $H_2$-TPR, UV-vis and $N_2$ adsorption-desorption techniques.

# Experimental

## 2.1 Preparation of the catalysts

Five copper loaded η-alumina catalysts Cu(x)-$Al_2O_3$, with x theoretical copper loadings were prepared by wet impregnation/evaporation technique. In a flask containing 100 mL of distilled water, the desired amount of copper acetate $Cu(CO_2CH_3)_2.H_2O$ was added to obtain the copper contents of 1 wt.%, 2 wt.%, 3wt.%, 5 wt.% and 7.5 wt%. After the total dissolution of the copper acetate, a mass of 1.5 g of alumina η-$Al_2O_3$ was added. The flask is then mounted on a rotary evaporator and the suspension is stirred for 4 hours at 80 ° C. After this step, the water was evaporated under reduced pressure for about 1 hour. Once dry, the solid was placed in an oven at 80°C overnight and finally calcined at 500°C under an air stream (2°C/min) for 10 hours. In Fig. 1 are reported the photographs of the prepared catalysts.

## 2.2 Characterization of Cu(x)-$Al_2O_3$ catalysts

X-ray powder diffraction patterns were obtained using a D8 ADVANCE BRUKER 40 Kv 40 mA Detector Lynx eye Geometrie Bragg Brenterno (ICGM MAES) using Cu Kα (λ = 0.15418 nm) incident radiation. The diffractograms were recorded at room temperature (RT) between 4° and 70 ° counted in 2θ at a scan speed of 0.02°/s.

The textural properties, surface area and porosity of the support and the catalysts were determined from nitrogen adsorption–desorption isotherms measured at -196°C using the “micrometrics Tristar Surface Area and Porosity analyzer”. The sample (approximately 100 mg) was weighed exactly in a glass tube lined with an "insert" to reduce the void volume. Before all measurements, the samples were treated under high vacuum overnight at 150°C.

$H_2$-TPR profiles were carried out with an automated Micromeritics Autochem 2910 analyzer. Before $H_2$-TPR measurements, samples (50 mg) were pretreated in a quartz U-tube reactor under 5%$O_2$/He flow (30 $cm^3$/min) at 550°C (10°C/min) for 30 min and then cooled under helium to 60°C. The samples were then reduced from 60°C to 800°C (5°C/min) under 3% $H_2$/Ar atmosphere (30 $cm^3$/min). The reduction gas $H_2$/Ar, was passed after the reactor through a freezing trap (propan-2-ol + liquid nitrogen) kept at -80°C to remove the formed water. Hydrogen consumption was monitored continuously by a thermal conductivity detector.

The ammonia desorption programmed as a function of the temperature ($NH_3$-TPD) was carried out using the same $H_2$-TPR equipment. A mass of 30 mg of catalyst is pretreated at 450°C for 30 min, under air flow (30 $cm^3$/min), then saturated with ammonia at 100°C and purged with helium for 45 min. Following this adsorption, the physisorbed ammonia is removed by leaving the sample for 2 h at 100°C, under a helium flow rate of 30 $cm^3$/min. Finally, the temperature was raised to 550°C (10°C/min), under a helium flow rate of 30 $cm^3$/min.

The Selective Catalytic Reduction of NO by $NH_3$ was carried out in a fixed-bed quartz flow reactor operating at atmospheric pressure. The catalyst (24 mg) was activated in-situ at 550°C for 1 hour under a flow of $O_2$/He (20/80, v/v) and then cooled to 180°C. A feed mixture of 1000 ppm NO, 1000 ppm $NH_3$, 8% $O_2$ in He and 3.5% $H_2O$ was then passed through the catalyst at a flow rate of 100 $cm^3$/min (VVH = 250000 $cm^3$/g. h). The $NH_3$-SCR was carried out on programmed temperature from 180°C to 500°C with the heating rate of 5°C/min.

For the Selective Catalytic Oxidation of ammonia ($NH_3$-SCO), the test was carried out on the catalysts already tested in the $NH_3$-SCR of NO. At 550°C, the NO flow is cut off and the $NH_3$-SCO experiments were carried out adjusting He flow and by decreasing the temperature from 500°C to 180°C with the heating rate of 5°C/ min.

The reactants and products were analysed by a quadruple mass spectrometer (Pfeiffer Omnistar) equipped with Channeltron and Faraday detectors (0–200 amu) following these characteristic masses: NO (30), $N_2$ (14, 28), $N_2O$ (28, 30, 44), $NH_3$ (15, 17, 18), $O_2$ (16, 32) and $H_2O$ (17, 18).

The percentages of NO ($X_{NO}$) and $NH_3$ ($X_{NH3}$) conversions were calculated on the basis of the differences in their concentrations measured before and after the catalyst bed.

$$X_{NO} = \frac{(NO)_0 - (NO)_T}{(NO)_0} \times 100$$

$$X_{NH_3} = \frac{(NH_3)_0 - (NH_3)_T}{(NH_3)_0} \times 100$$

## Results And Discussion

# 3.1 Characterization of the catalysts

The XRD patterns of the support η-$Al_2O_3$, CuO (Sigma Aldrich, ACS reagent ≥ 99.0 %) and the prepared catalysts Cu(x)-$Al_2O_3$ are shown in **Fig. 2.** The characteristic peaks at angles in 2θ 19.5°, 37.5°, 39.7°, 45.8°, 60.8° and 67.2° correspond to η-$Al_2O_3$ phase having spinel lattice (JCPDS, No. 04-0875). The introduction of copper leads to the destruction of the structure of η-$Al_2O_3$ for the catalysts with higher copper contents Cu(3)-$Al_2O_3$, Cu(5)-$Al_2O_3$ and Cu (7.5) -$Al_2O_3$. These catalysts showed the characteristic peaks of CuO (JCPDS, No. 80 – 0076) at the angles in 2θ 32.6°, 35.6°, 38.8° and 48.8°, 58.3° and 61.5° (Liang et al., 2012). On the other hand, for the Cu(1)-$Al_2O_3$ and Cu(2)-$Al_2O_3$ catalysts, there is a slight decrease in the intensity of the peaks of the support and particularly the peak at 19.5 ° and the absence of the diffraction peaks of CuO. It appears that the copper species present in the Cu(1)-$Al_2O_3$ and Cu (2)-$Al_2O_3$ catalysts are small and well dispersed on the surface of the support. Friedman et al. (Friedman et al., 1978) showed that the saturation of the CuO/ γ-$Al_2O_3$ catalyst surface a CuO monolayer occurs for a

Cu content of about 4–5% by weight for every 100 $m^2/g$ of alumina. Beyond this threshold, crystalline CuO was observed.

The SEM micrographs of the η-$Al_2O_3$ and the catalysts Cu(2)-$Al_2O_3$ and Cu(3)-$Al_2O_3$ are illustrated in **Fig. 3.** The SEM micrograph of alumina η-$Al_2O_3$ is made up small agglomerate particles. The introduction of copper leads to a change in the morphology of η-$Al_2O_3$ particles. For example, the Cu(2)-$Al_2O_3$ catalyst presents a sponge-like morphology, which reveals a high level of porosity. On the other hand, for the Cu(3)-$Al_2O_3$ catalyst, one can see two phases. The first one is relative to sintered alumina particles and the second is related to CuO particles. It appears that high levels of copper favor the sintering of alumina at lower temperatures than usual. Sintering leads to the drop of the specific surface and the deterioration of the dispersion state of the copper species on the surface of the support.

The TEM images of the Cu(1)-$Al_2O_3$, Cu(2)-$Al_2O_3$ and Cu(3)-$Al_2O_3$ catalysts are reported in **Figs. 4.** For (Cu(1)-$Al_2O_3$ catalyst, we note that the copper particles are very small and well dispersed on the support η-$Al_2O_3$. The increase of the amount of copper leads to the increase of copper species size. For Cu(2)-$Al_2O_3$ catalyst, copper particles have size about 5–10 nm. Whereas for the Cu(3)-$Al_2O_3$ catalyst, we note the presence of black spherical particles exceeding 70 nm attributed to copper oxide CuO as shown by XRD.

Textural properties of the support η-$Al_2O_3$ and the prepared catalysts Cu(x)-$Al_2O_3$ are presented in **Table 1** and **Fig. 5.** It is noted that the $S_{BET}$ of the catalysts decrease after the wet impregnation/evaporation with copper acetate. For example, the specific surface area of the support ($S_{BET}$ = 417 $m^2/g$) decreases by 18% when 1% of copper was added ($S_{BET}$ = 343 $m^2/g$) and 60% with the higher content of copper 7.5% ($S_{BET}$ = 169. $m^2/$ g). Indeed, the XRD have shown that Cu(3)-$Al_2O_3$, Cu(5)-$Al_2O_3$ and Cu(7.5)-$Al_2O_3$ catalysts contain large CuO particles which block the porous structure of η-$Al_2O_3$. On the other hand, for Cu(1)-$Al_2O_3$ and Cu (2)-$Al_2O_3$ catalysts the copper species are well dispersed on the surface of the support and the decrease of $S_{BET}$ was moderate (only 16% for Cu(2)-$Al_2O_3$ catalyst). On the other hand, we notice an increase in the pore volume up to a copper quantity of 2% wt. and then a decrease beyond this value. Actually, the pore volume of the support which was Vp = 0.295 $cm^3/g$ increases by about 30% (Vp = 0.387 $cm^3/g$) for 1% Cu and 40% (Vp = 0.411$cm^3/$ g) for 2% Cu. This result could explain the morphology of η-$Al_2O_3$ and the formation of macropores as shown by SEM technique. On the other hand, increasing the copper content from 3–7.5% induces a reduction in the pore volumes of the catalysts due to the sintering of η-$Al_2O_3$ particles.

In **Fig. 5** are reported the $N_2$ adsorption-desorption isotherms of η-$Al_2O_3$ and Cu(x)-$Al_2O_3$ catalysts. All adsorption isotherms are of type IV having hysteresis loops characteristics for mesoporous solids (Petitto et al.,2013). Nevertheless, we note that the addition of copper to the η-$Al_2O_3$ changes the hysteresis loop from H3 to H2(b) type. This behavior could reflect a change in the pore shape and distribution with the introduction of copper. Indeed, H3 type hysteresis loop indicates the presence of narrow slit-like pores

particles with internal voids of irregular shape and broad size distribution but the H2(b) hysteresis loop type shows a narrow distribution of pore shape with a wide neck size distribution (Cychosz and Thommes, 2018). Likewise, when the amount of copper increases there is a decrease in the adsorbed volume at low relative pressure (P/P°), indicating the decrease in microporosity and the increase in mesoporosity.

Table 1
Textural parameters of the prepared catalysts Cu(x)-$Al_2O_3$

| Sample | $S_{BET}$ ($m^2$/g) | BJH Pore volume ($cm^3$/g) | BJH pore diameter (nm) |
| --- | --- | --- | --- |
| η-$Al_2O_3$ | 417 | 0.295 | 4.50 |
| Cu(1)-$Al_2O_3$ | 343 | 0.387 | 4.79 |
| Cu(2)-$Al_2O_3$ | 351 | 0.411 | 4.85 |
| Cu(3)-$Al_2O_3$ | 226 | 0.319 | 4.27 |
| Cu(5)-$Al_2O_3$ | 229 | 0.229 | 4.67 |
| Cu(7.5)-$Al_2O_3$ | 169 | 0.165 | 4.69 |

$H_2$-TPR profiles of the studied samples are shown in **Fig. 6.** It is observed that Cu(1)-$Al_2O_3$ and Cu(2)-$Al_2O_3$ catalysts have similar reduction profiles **(Fig. 7)**. With the increase of copper amount there is an increase of the intensity of the peaks. For Cu(2)-$Al_2O_3$ catalyst, the first peak around 130°C was attributed according to Yan et al., 1996 to the reduction of well dispersed CuO clusters on the surface of the support. The second peak extending from 300°C to 500°C corresponds to the reduction of highly dispersed $Cu^{2+}$ cations in the structure of the alumina forming a surface spinel $CuAl_2O_4$ type (Aguila et al., 2008; Il'chenko et al., 1976). On the other hand, when the copper content was increased above 3 wt%, there are changes in the catalyst reduction profiles. Indeed, Cu(3)-$Al_2O_3$, Cu(5)-$Al_2O_3$ and Cu(7.5)-$Al_2O_3$ profiles show single reduction peaks centered in a temperature range of 140–380°C **(Fig. 8)**. The extent of the peaks could indicate the existence of different CuO species with different sizes and environments. Fierro et al., 1994 reported that the supported CuO particle reduction temperature range extends from 200 to 300°C depending on the type of support. For the Cu(3)-$Al_2O_3$ catalyst, the peak ranges from 170 to 375°C and the temperature where the reduction rate is maximum is around 242°C.

The deconvolution of the reduction profile of the Cu (3) -$Al_2O_3$ catalyst is shown in **Fig. 9.** The results of deconvolution of the $H_2$-TPR profiles of the Cu(3)-$Al_2O_3$,Cu(5)-$Al_2O_3$ and Cu(7.5)-$Al_2O_3$ catalysts are reported in **Table 2.**

For Cu(3)-$Al_2O_3$, the central peak was deconvolved into three peaks. The first is located around 209°C with a relative surface area of around 11%, the second around 232°C (15%) and the last around 274°C

(74%). It is noted that the majority of CuO particles are reduced at high temperature because of their large size.

Table 2
Results of deconvolution of the $H_2$-TPR profiles of the Cu(3)-$Al_2O_3$, Cu(5)-$Al_2O_3$ et Cu(7.5)-$Al_2O_3$ catalysts

| catalysts | Maximum reduction temperature $T_m$ (°C) | | |
|---|---|---|---|
| | Pic I | Pic II | Pic III |
| **Cu(3)-$Al_2O_3$** | 209 (11%) | 232 (15%) | 274 (74%) |
| **Cu(5)-$Al_2O_3$** | - | 220 (46%) | 282 (54%) |
| **Cu(7.5)-$Al_2O_3$** | 179 (11%) | 222 (41%) | 268 (48%) |

The nature and environment of copper species present in the prepared catalysts have been studied by UV-vis spectroscopy. The UV-vis spectra of the carrier η-$Al_2O_3$ and the Cu(x)-$Al_2O_3$ catalysts are shown in **Fig. 10.** Generally, alumina is transparent in the UV-visible range. Nevertheless, the absorption band around 370 nm of support that could be attributed to impurities. The spectra of the Cu(1)-$Al_2O_3$ and Cu(2)-$Al_2O_3$ catalysts have the same profile characterized by a broad absorption band that extends from 350 to 650 nm and centered around 490 nm. This band could be attributed according to the literature (Chaudhary et al., 2018; Buvaneswari, 2015) to CuO or surface spinel type $CuAl_2O_4$ species. The catalysts Cu(3)-$Al_2O_3$, Cu(5)-$Al_2O_3$ and Cu(7.5)-$Al_2O_3$ exhibit characteristic spectra of well-crystallized CuO.

The $NH_3$-TPD profiles of η-$Al_2O_3$ and the prepared Cu(x)-$Al_2O_3$ catalysts are reported in **Fig. 11.** The support η-$Al_2O_3$ has broad ammonia desorption peak which extends from 110°C to 475°C with a maximum at around 180°C. The catalysts Cu(1)-$Al_2O_3$ and Cu (2)-$Al_2O_3$ show similar desorption profiles to the support but with a higher intensity of the peaks. For the other catalysts Cu(3)-$Al_2O_3$, Cu(5)-$Al_2O_3$ and Cu(7.5)-$Al_2O_3$, the appearance of a peak around 300°C is observed which increases in intensity with the increase of the copper amounts. Generally, the temperature of desorbed ammonia is related to the strength of acidic sites in the samples. So, according to the maximum desorption temperature of ammonia ($T_d$) (Carre et al., 2010), there are three types of acidic sites: *i)* weak acidic sites ($150 \leq T_d$ (°C) $\leq 250$), *ii)* average acidic sites ($250 < T_d$ (°C) $\leq 350$) *iii)* strong acidic sites $T_d$ (°C) $> 350$. The $NH_3$ desorption at $T \leq 150$°C could be attributed to the $NH_3$ molecules weakly bound to the surface of the support which have not been evacuated at 100°C.

# 3.2 Evaluation of the catalytic activity of Cu(x)-$Al_2O_3$ catalysts

### *3.2.1 Selective Catalytic Reduction of NO by $NH_3$*

The prepared catalysts were tested in the $NH_3$-SCR of NO in the presence of an excess of oxygen and of water vapor according to reaction (I):

**$4NO + 4NH_3 + O_2 \rightarrow 4 N_2 + 6H_2O$ (I)**

In **Figs. 12** and **13** are reported the NO conversion and $NH_3$ conversion of the prepared Cu(x)-$Al_2O_3$ catalysts in the $NH_3$-SCR of NO. The NO conversion increased initially with increasing temperature, then reached a maximum and decreased. The evolution of the NO conversion passing through a maximum reflects the existence of a competition between two reactions; the first concerning the reduction of NO and the second the oxidation of $NH_3$ by the oxygen present in the gas mixture. The competition between the two reactions is in favor of the oxidation of $NH_3$ at high temperatures which explains the decline in NO conversion. The decrease in the NO conversion is also accompanied with some formation of $N_2O$ according to the two non-selective reactions II and III:

**$2NH_3 + 2O_2 \rightarrow 2N_2O + 3H_2O$ (II)**

**$4NH_3 + 4NO + 3O_2 \rightarrow 4N_2O + 6H_2O$ (III)**

Cu(1)-$Al_2O_3$ and Cu(2)-$Al_2O_3$ catalysts have similar NO and $NH_3$ conversion profiles up to 475°C. Beyond this temperature, the NO conversion decreases for the Cu(2)-$Al_2O_3$ catalyst, whereas it continues to increase for Cu(1)-$Al_2O_3$ up to 500°C where a maximum NO conversion is about 91%. If we look to the conversion of NO to $N_2$, we notice that these two catalysts are almost selective towards $N_2$ (**Fig. 14**), due to the fact that the oxidation of $NH_3$ is less favored due to the better dispersion of copper. The others catalysts, (Cu(3)-$Al_2O_3$, Cu(5)-$Al_2O_3$ and Cu(7.5)-$Al_2O_{3,}$ display a volcano-shape curve of NO conversion as temperature increases while $NH_3$ conversion continue to increase with the temperature. For example (Fig. 12), the catalyst Cu(7.5)-$Al_2O_3$ has a maximum NO conversion of the order of 40% at 350°C which is accompanied with small $N_2O$ production. Therefore, the large drop in NO conversion on this catalyst above 350°C is due to the $NH_3$ oxidation into NO. Moreover, above 425°C, no NO reduction by ammonia occurs since NO concentration in the outlet gas is superior at the NO concentration in the inlet gas. The behavior of these catalysts could be related to the presence of large CuO particles. One can conclude that the two catalysts Cu(1)-$Al_2O_3$ and Cu (2)-$Al_2O_3$ are the most efficient in the reduction of NO by $NH_3$ in the presence of 3.5% of water vapor. Nevertheless, the Cu(1)-$Al_2O_3$ has a slightly better NO reduction behaviour at high temperature. It has been found that the high NO conversion of these two catalysts can be related to the presence of small CuO clusters deposited on the surface of η-$Al_2O_3$ alumina and to $CuAl_2O_4$ surface spinel. We believe that small CuO clusters deposited on the surface and easily reduced at low temperatures are responsible for high temperature $N_2$ selectivity. In fact, according to the $H_2$-TPR results, the quantity of these copper species is greater in the case of Cu(2)-$Al_2O_3$ the and Cu(1)-$Al_2O_3$ catalysts.

Kwak et al., 2012 investigated the $NH_3$-SCR of NO reaction under lean conditions on CuO-γ-$Al_2O_3$ catalysts. They showed that on 10 wt % CuO/γ-$Al_2O_3$, the NOx conversion is about 30% at 350°C and $NH_3$ reacts primarily with oxygen to produce NOx. However, on a 0.5 wt CuO/γ$Al_2O_3$ catalyst, $NH_3$ reacts with NO to form $N_2$ and the NOx conversion to $N_2$ was almost 80% at 450°C.

### *3.2.2 Selective catalytic Oxidation of $NH_3$*

The oxidation profiles of $NH_3$ in the presence of 3.5% water vapor of the prepared catalysts Cu(x)-$Al_2O_3$ are presented in **Fig. 15.** The studied reaction is as follows (IV):

**$4NH_3 + 3O_2 \rightarrow 2N_2 + 6H_2O$ (IV)**

For all catalysts, it is noted that ammonia oxidation increases with the increase in temperature. For the Cu(3)-$Al_2O_3$, Cu (5)-$Al_2O_3$ and Cu(7.5)-$Al_2O_3$ catalysts, a gradual increase in $NH_3$ oxidation from 200°C to 400°C was recorded. But above 400°C, the oxidation of $NH_3$ decreases slightly. On the other hand, for Cu(1)-$Al_2O_3$ and Cu(2)-$Al_2O_3$ a gradual slower increase of the $NH_3$ conversion was recorded from 250 ° C to 550 ° C. These two catalysts are much less active towards ammonia oxidation as we have already seen previously in $NH_3$-SCR of NO. The catalytic activity of the catalyst Cu(1)-$Al_2O_3$ and Cu(2)-$Al_2O_3$ in the oxidation of $NH_3$ could be related to the highly dispersed CuO on the support which are reduced at low temperature T = 130°C. According to Gang et al., 2000; 1999 complete oxidation of $NH_3$ was obtained at 350°C on Cu(10%)-γ$Al_2O_3$ catalyst with $N_2$ selectivity of 90%. Liang et al., 2012 obtained similar results for Cu(10%)-γ$Al_2O_3$ catalysts prepared by different copper precursors (nitrate, acetate and sulfate) and calcined at 500°C and 600°C. They showed that a mixture of CuO and $CuAl_2O_4$ species is formed on the various Cu(10%)-γ$Al_2O_3$ catalysts. On the other hand, the dispersion and the nature of the copper species have a significant influence on the activity of the catalysts. Indeed, the highly dispersed CuO nanoparticles on the support are responsible for the high activity of Cu(10%)-γ$Al_2O_3$ catalysts. Lenihan and Curtin (2009) using lower levels of copper (Cu(3.4%)/γ-$Al_2O_3$) found conversions of the order of 100% in $NH_3$.

The nature of the copper precursor and the method of preparation were found to be determinants in the formation of active copper species in the $NH_3$-SCO. For example, a sulphate precursor leads to the formation of $CuAl_2O_4$, whereas CuO of higher crystallinity is formed using an acetate compared to a nitrate precursor (Jung et al., 2017). However, the nature of the active species in $NH_3$- SCO has not been fully verified yet. Gang et al., 2000 claimed that the surface $CuAl_2O_4$ spinel phase is responsible for the higher catalytic activity relative to CuO. A study conducted by Liang et al., 2012 has shown that a mixture of CuO and $CuAl_2O_4$ phases is formed on the various Cu (10%) - γ$Al_2O_3$ catalysts. On the other hand, the dispersion and the nature of the copper species have a significant influence on the activity of the catalysts. Indeed, CuO nanoparticles highly dispersed on the support and easily reduced at low temperature are responsible for the high conversion of $NH_3$.

**Figure 16, 17 and Fig. 18** presents the selectivity profiles towards NO, $N_2O$ and $N_2$ respectively obtained in the $NH_3$-SCO reaction. $N_2$ is the desired gas product, while NO and $N_2O$ are undesired by-products. The Cu(1)-$Al_2O_3$ and Cu(2)-$Al_2O_3$ catalyst has $N_2$ selectivity close to 95% over the temperature range of 200–400°C. Additionally, the transition metal oxides have been widely studied in the scientific literature (Jablonska and Palkovits, 2016; Sazonova et al., 1996). This type of catalysts showed higher selectivity to $N_2$, however, they need significantly higher operation temperatures as high as 300–500 ∘C than noble metal catalysts. For the three others Cu(x)-$Al_2O_3$, selectivities towards $N_2$ are much lower. At 550°C (**Fig. 16**), 48%, 40%, 30% of selectivity towards NO were measured for (Cu(7.5)-$Al_2O_3$, Cu(5)-$Al_2O_3$, Cu(3)-$Al_2O_3$) respectively.

The $NH_3$-SCO method is an effective method for oxidizing $NH_3$ into $N_2$. The overall selectivity into $N_2$ was close to 100% for Cu(1)-$Al_2O_3$ and above 95% for Cu(2)-$Al_2O_3$ over all the temperature while for the other three catalysts, $N_2$ selectivity remains as high as 95% only at temperature below 350°C, as reported by Jabłońska et al.,2017; 2018. Highly dispersed CuOx favor moderate activity but $N_2$ selectivity up to 550°C in $NH_3$-SCO (Chmielarz et al., 2005). In a similar work, Dong et al. (2013) showed that nitrogen gas was primarily formed by the direct dissociation of the NO produced by the oxidation of the adsorbed $NH_3$ (Dong et al., 2014).

# Conclusion

Copper-supported η-$Al_2O_3$ catalysts have prepared and tested in the selective catalytic reduction of NO by $NH_3$ and in the selective catalytic oxidation of $NH_3$.The impregnation/evaporation method has successfully dispersed the copper species on the surface of the alumina for the low copper contents; Cu(1)-$Al_2O_3$ and Cu(2)-$Al_2O_3$ catalysts. The XRD showed that the introduction of an additional amount of copper leads to the destruction of the alumina structure when copper content exceeded 3% wt.%. The Cu(3)-$Al_2O_3$, Cu(5)-$Al_2O_3$ and Cu (7.5) -$Al_2O_3$ catalysts contain mainly large CuO particles. Cu(2)-$Al_2O_3$ and Cu(1)-$Al_2O_3$ catalysts have interesting NO conversion to $N_2$ in the $NH_3$-SCR of NO. This activity could be related essentially to the small CuO clusters deposited on the alumina surface and $CuAl_2O_4$ species. For $NH_3$-SCO, the catalyst Cu(1)-$Al_2O_3$ and Cu(2)-$Al_2O_3$ exhibit similar behavior resulting in the conversion of $NH_3$ to $N_2$ of about 100% at T > 500 ° C. This conversion could be attributed to CuO nanoparticles highly dispersed on the support and easily reduced at low temperature.

# Declarations

**Ethics approval and consent to participate** “Not applicable.

**Consent for publication** “Not applicable”.

**Competing interests** The authors declare that they have no known competing financial interests or personal relationships that could have appeared to influence the work reported in this paper.

**Availability of data and materials** “Not applicable”.

**Funding** “Not applicable”.

**Authors' contributions**

Nawel Jraba: analyzed the data and write the complete paper.

HassibTounsi, Thabet Makhlouf  and Gerard Delahay: gave this idea of work.

All authors read and approved the final manuscript.

# References

1. Águila G, Gracia F, Araya P (2008) CuO and CeO2 catalysts supported on $Al_2O_3$, $ZrO_2$, and $SiO_2$ in the oxidation of CO at low temperature. Appl Catal A 343(1-2):16–24. https://doi.org/10.1016/j.apcata.2008.03.015
2. Boroń P, Rutkowska M, Gil B, Marszałek B, Chmielarz L, Dzwigaj S (2019) Experimental Evidence of the Mechanism of Selective Catalytic Reduction of NO with NH3 over Fe-Containing BEA Zeolites. Chem Sus Chem 12.3:692–705. https://doi.org/10.1002/cssc.201801883
3. Buvaneswari G, Aswathy V, Rajakumari R (2015) Comparison of color and optical absorbance properties of divalent ion substituted Cu and Zn aluminate spinel oxides synthesized by combustion method towards pigment application. Dyes Pigm 123:413–419. https://doi.org/10.1016/j.dyepig.2015.08.024
4. Carre S, Tapin B, Gnep NS, Revel R, Magnoux P,. Magnoux (2010) Model reactions as probe of the acid–base properties of aluminas: Nature and strength of active sites. Correlation with physicochemical characterization. Appl Catal A 372(1):26–33. https://doi.org/10.1016/j.apcata.2009.10.005
5. Chaudhary RG, Sonkusare VN, Bhusari GS, Mondal A, Shaik DP, Juneja HD (2018) Microwave-mediated synthesis of spinel $CuAl_2O_4$ nanocomposites for enhanced electrochemical and catalytic performance. Res Chem Intermediat 44.3:2039–2060. https://doi.org/10.1007/s11164-017-3213-z
6. Chmielarz L, Kuśtrowski P, Rafalska-Łasocha A, Dziembaj R (2005) Selective oxidation of ammonia to nitrogen on transition metal containing mixed metal oxides. Appl Catal B Environ 58:235–244. https://doi.org/10.1016/j.apcatb.2004.12.009
7. Cychosz KA, Thommes M (2018) Progress in the physisorption characterization of nanoporous gas storage materials. Eng 44, 559–566. https://doi.org/10.1016/j.eng.2018.06.001
8. Damma D, Ettireddy PR, Reddy BM, Smirniotis PG (2019) A review of low temperature $NH_3$-SCR for removal of NOx. Catalysts 9(4):349. https://doi.org/10.3390/catal9040349
9. Dong CD, Chen CW, Hung CM (2014) Catalytic performance and characterization of copper-based Rare earth composite materials for selective catalytic oxidation reaction with simulated synthetic

ammonia stream. Journal of Advanced Oxidation Technologies 17(2):352–358. https://doi.org/10.1515/jaots-2014-0220

10. Fierro G, Lojacono M, Inversi M, Porta P, Lavecchia R, Cioci F (1994) A study of anomalous temperature-programmed reduction profiles of $Cu_2O$, CuO, and CuO-ZnO catalysts. J Catal 148.2:709–721. https://doi.org/10.1006/jcat.1994.1257
11. Forzatti P (2001) Present status and perspectives in de-NOx SCR catalysis. Appl Catal A 222:221–236. https://doi.org/10.1016/S0926-860X(01)00832-8
12. Friedman RM, Freeman JJ, Lytle FW (1978) Characterization of CuAl2O3 catalysts. J Catal 55.1:10–28. https://doi.org/10.1016/0021-9517(78)90181-1
13. Gang L, Anderson BG, Van Grondelle J, Van Santen RA (2000) $NH_3$ oxidation to nitrogen and water at low temperatures using supported transition metal catalysts. Catal Today 61(1-4):179–185. https://doi.org/10.1016/S0920-5861(00)00375-8
14. Gang L, Van Grondelle J, Anderson BG, Van Santen RA (1999) Selective low temperature NH3 oxidation to N2 on copper-based catalysts. J Catal 186.1:100–109. https://doi.org/10.1006/jcat.1999.2524
15. Gao F, Szanyi J (2018) On the hydrothermal stability of Cu/SSZ-13 SCR. Appl Catal A 560:185–194. https://doi.org/10.1016/j.apcata.2018.04.040
16. Ghosh RS, Le TT, Terlier T, Rimer JD, Harold MP, Wang D (2020) Enhanced Selective Oxidation of Ammonia in a Pt/$Al_2O_3$@Cu/ZSM-5 Core–Shell Catalyst. ACS Catal 106, 3604–3617. https://doi.org/10.1021/acscatal.9b04288
17. Goldbach M, Roppertz A, Langenfeld P, Wackerhagen M, Füger S, Kureti S (2017) Urea decomposition in selective catalytic reduction on V2O5/WO3/TiO2 catalyst in diesel exhaust. Chem Eng Technol 40(11):2035–2043. https://doi.org/10.1002/ceat.201700261
18. Hamoud HI, Valtchev V, Daturi M (2019) Selective catalytic reduction of NOx over Cu-and Fe-exchanged zeolites and their mechanical mixture. Appl Catal B 250:419–428. https://doi.org/10.1016/j.apcatb.2019.02.022
19. Hansen TK, Høj M, Hansen BB, Janssens TV, Jensen AD (2017) The Effect of Pt Particle Size on the Oxidation of CO, C 3 H 6, and NO Over Pt/$Al_2O_3$ for Diesel Exhaust Aftertreatment. Top Catal 6017-18, 1333–1344. https://doi.org/10.1007/s11244-017-0818-9
20. Il'chenko, Ivanovna N (1976) Catalytic oxidation of ammonia. Russian Chemical Reviews. 45.12, 1119. https://doi.10.1070/RC1976v045n12ABEH002765
21. Jabłońska M (2020) Progress on Selective Catalytic Ammonia Oxidation (NH3-SCO) over Cu – Containing Zeolite-Based. Catalysts ChemCatChem 12(18):4490–4500. https://doi.org/10.1002/cctc.202000649
22. Jabłońska M, Beale AM, Nocuń M, Palkovits R (2018) Ag-Cu based catalysts for the selective ammonia oxidation into nitrogen and water vapour. Applied Catalysis B: Environmental 232:275–287. https://doi.org/10.1016/j.apcatb.2018.03.029

23. Jabłońska M, Wolkenar B, Beale AM, Pischinger S, Palkovits R (2018) Comparison of Cu-Mg-Al-Ox and Cu/Al2O3 in selective catalytic oxidation of ammonia (NH3-SCO). Catal Commun 110:5–9. https://doi.org/10.1016/j.catcom.2018.03.003
24. Jabłońska M, Nocuń M, Gołąbek K, Palkovits R (2017) Effect of preparation procedures on catalytic activity and selectivity of copper-based mixed oxides in selective catalytic oxidation of ammonia into nitrogen and water vapour. Appl Surf Sci 423:498–508. https://doi.org/10.1016/j.apsusc.2017.06.144
25. Jabłońska M, Palkovits R (2016) Copper based catalysts for the selective ammonia oxidation into nitrogen and water vapour—recent trends and open challenges. Appl Catal B 181:332–351. https://doi.org/10.1016/j.apcatb.2015.07.017
26. Jabłońska M (2015) Selective catalytic oxidation of ammonia into nitrogen and water vapour over transition metals modified Al 2 O 3, TiO 2 and ZrO 2. Chem Pap 69.9:1141–1155. https://doi.org/10.1515/chempap-2015-0120
27. Jeong SM, Jung SH, Yoo KS, Kim SD (1999) Selective catalytic reduction of NO by $NH_3$ over a bulk sulfated CuO/γ-$Al_2O_3$ catalyst. Ind Eng Chem Res 38.6:2210–2215. https://doi.org/10.1021/ie9807147
28. Jraba N, Tounsi H, Makhlouf T (2018) Valorization of aluminum chips into γ-$Al_2O_3$ and η-$Al_2O_3$ with high surface areas via the precipitation route. Waste Biomass Valori 9.6:1003–1014. https://doi.org/10.1007/s12649-016-9786-8
29. Jung Y, Shin YJ, Pyo YD, Cho CP, Jang J, Kim G (2017) NOx and $N_2O$ emissions over a Urea-SCR system containing both $V_2O_5$-$WO_3$/$TiO_2$ and Cu-zeolite catalysts in a diesel engine. Chem Eng J 326:853–862. https://doi.org/10.1016/j.cej.2017.06.020
30. Kong T, Jia Y, Zhang L, Shu H, Chang X, Kuang W, Luo M (2020) CuO−MoO2−CeO2 yolk−albumen−shell catalyst supported on γ-Al 2 O 3 for denitration with resistance to $SO_2$. J Mater Sci 559, 3833–3844. https://doi.org/10.1007/s10853-019-04216-x
31. Kröcher O (2018) Selective catalytic reduction of NOx. 459. https://doi.org/10.3390/catal8100459
32. Kwak JH, Tonkyn R, Tran D, Mei D, Cho SJ, Kovarik L, … Szanyi J (2012) Size-dependent catalytic performance of CuO on γ-$Al_2O_3$: NO reduction versus $NH_3$ oxidation. ACS Catal 27, 1432–1440. https://doi.org/10.1021/cs3002463
33. Lai JK, Wachs IE (2018) A perspective on the selective catalytic reduction (SCR) of NO with NH3 by supported $V_2O_5$–$WO_3$/$TiO_2$ catalysts. ACS Catal 8.7:6537–6551. https://doi.org/10.1021/acscatal.8b01357
34. Lambert CK (2019) Perspective on SCR NO x control for diesel vehicles. *React* Chem Eng 4(6):969–974. https://doi.org/10.1016/j.apcata.2018.04.040
35. Liang C, Li X, Qu Z, Tade M, Liu S (2012) The role of copper species on Cu/γ-$Al_2O_3$ catalysts for $NH_3$–SCO reaction. Appl Surf Sci 258.8:3738–3743. https://doi.org/10.1016/j.apsusc.2011.12.017

36. Lenihan S, Curtin T (2009) The selective oxidation of ammonia using copper-based catalysts: The effects of water. Catal Today 1451-2, 85–89. https://doi.org/10.1016/j.cattod.2008.06.017
37. Nova I, Tronconi E (eds)., 2014. Urea-SCR technology for deNOx after treatment of diesel exhausts. N. Y. Springer. 5. https://doi.org/10.1007/978-1-4899-8071-7
38. Panahi PN, Delahay G (2017) Activity of γ–$Al_2O_3$-based Mn, Cu, and Co oxide nanocatalysts for selective catalytic reduction of nitric oxide with ammonia. Turk J Chem 41.2:272–281. https://doi.org/10.3906/kim-1605-50
39. Petitto C, Mutin HP, Delahay G (2013) Hydrothermal activation of silver supported alumina catalysts prepared by sol–gel method: Application to the selective catalytic reduction (SCR) of NOx by n-decane. Appl Catal B 134:258–264. https://doi.org/10.1016/j.apcatb.2013.01.018
40. Piumetti M, Bensaid S, Fino D, Russo N (2015) Catalysis in Diesel engine NOx aftertreatment: a review. Catal Struct React 1.4:155–173. https://doi.org/10.1080/2055074X.2015.1105615
41. Sazonova NN, Simakov AV, Nikoro TA, Barannik GB, Lyakhova VF, Zheivot VI, Ismagilov ZR, Veringa H (1996) React Kinet Catal Lett 57:71–79. https://doi.org/10.1007/BF02076122
42. Shibata G, Eijima W, Koiwai R, Shimizu KI, Nakasaka Y, Kobashi Y, … Kusaka J (2019) NH3-SCR by monolithic Cu-ZSM-5 and Cu-AFX catalysts: Kinetic modeling and engine bench tests. Catal Today 332:59–63. https://doi.org/10.1016/j.cattod.2018.06.023
43. Ström L, Carlsson PA, Skoglundh M, Härelind H (2018) Surface species and metal oxidation state during H2-assisted NH3-SCR of NOX over alumina-supported silver and indium. Catalysts 8(1):38. https://doi.org/10.3390/catal8010038
44. Sun M, Liu J, Song C, Ogata Y, Rao H, Zhao X, … Chen Y (2019) Different Reaction Mechanisms of Ammonia Oxidation Reaction on Pt/Al2O3 and Pt/CeZrO2 with Various Pt States. *ACS* Appl Mater *Interfaces* 11.26:23102–23111. https://doi.org/10.1021/acsami.9b02128
45. Svintsitskiy DA, Kibis LS, Stadnichenko AI, Slavinskaya EM, Romanenko AV, Fedorova EA, … Boronin AI (2020) Insight into the nature of active species of Pt/$Al_2O_3$ catalysts for low temperature $NH_3$ oxidation. Chem Cat Chem 12.3:867–880. https://doi.org/10.1002/cctc.201901719
46. Usberti N, Jablonska M, Di Blasi M, Forzatti P, Lietti L, Beretta A (2015) Design of a high-efficiency NH3-SCR reactor for stationary applications. A kinetic study of NH3 oxidation and NH3-SCR over V-based catalysts. Appl Catal B 179:185–195. https://doi.org/10.1016/j.apcatb.2015.05.017
47. Villamaina R, Nova I, Tronconi E, Maunula T, Keenan M (2019) Effect of the NH 4 NO 3 Addition on the Low-T NH 3-SCR Performances of Individual and Combined Fe-and Cu-Zeolite Catalysts. Emiss Control Sci Technol 54, 290–296. https://doi.org/10.1007/s40825-019-00140-3
48. Walker A (2016) Future challenges and incoming solutions in emission control for heavy duty diesel vehicles. Top Catal 598-9, 695–707. https://doi.org/10.1007/s11244-016-0540-z
49. Xie G, Liu Z, Zhu Z, Liu Q, Ge J, Huang Z (2004) Simultaneous removal of $SO_2$ and NOx from flue gas using a $CuO/Al_2O_3$ catalyst sorbent: II. Promotion of SCR activity by $SO_2$ at high temperatures. J Catal 224(1):42–49. https://doi.org/10.1016/j.jcat.2004.02.016

50. Xin Y, Li Q, Zhang Z (2018) Zeolitic materials for DeNOx selective catalytic reduction. Chem Cat Chem 10.1:29–41. https://doi.org/10.1002/cctc.201700854
51. Yan JY, Lei GD, Sachtler WMH, Kung HH (1996) Deactivation of Cu/ZSM-5 catalysts for lean NOx reduction: characterization of changes of Cu state and zeolite support. J Catal 161(1):43–54. https://doi.org/10.1006/jcat.1996.0160
52. Yuan X, Liu H, Gao Y (2015) Diesel engine SCR control: current development and future challenges, Emiss Control Sci Technol 12, 121–133. https://doi.org/10.1007/s40825-015-0013-z

## Figures

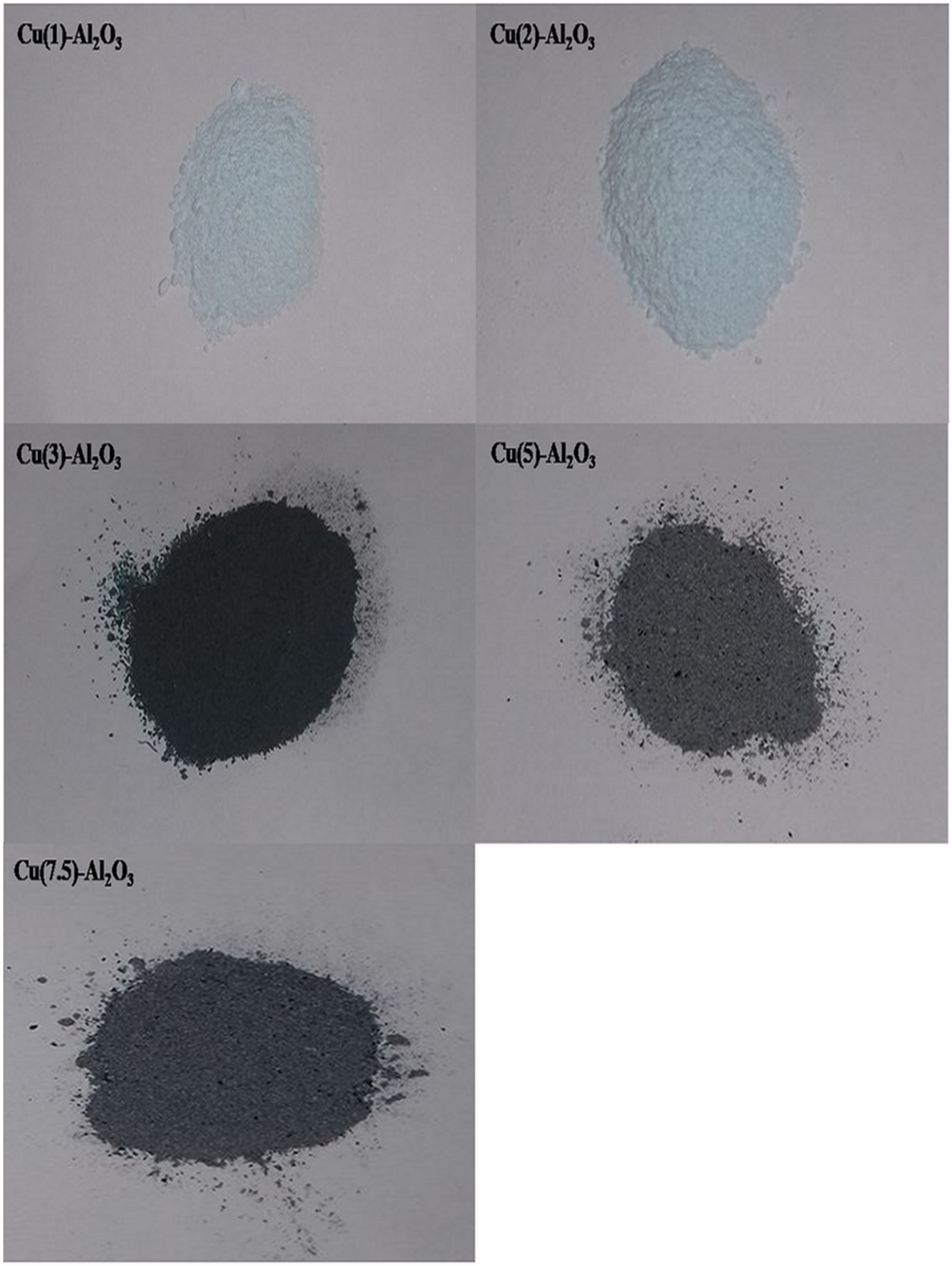


### Figure 1

Colors of the prepared catalysts after copper loading and calcination.

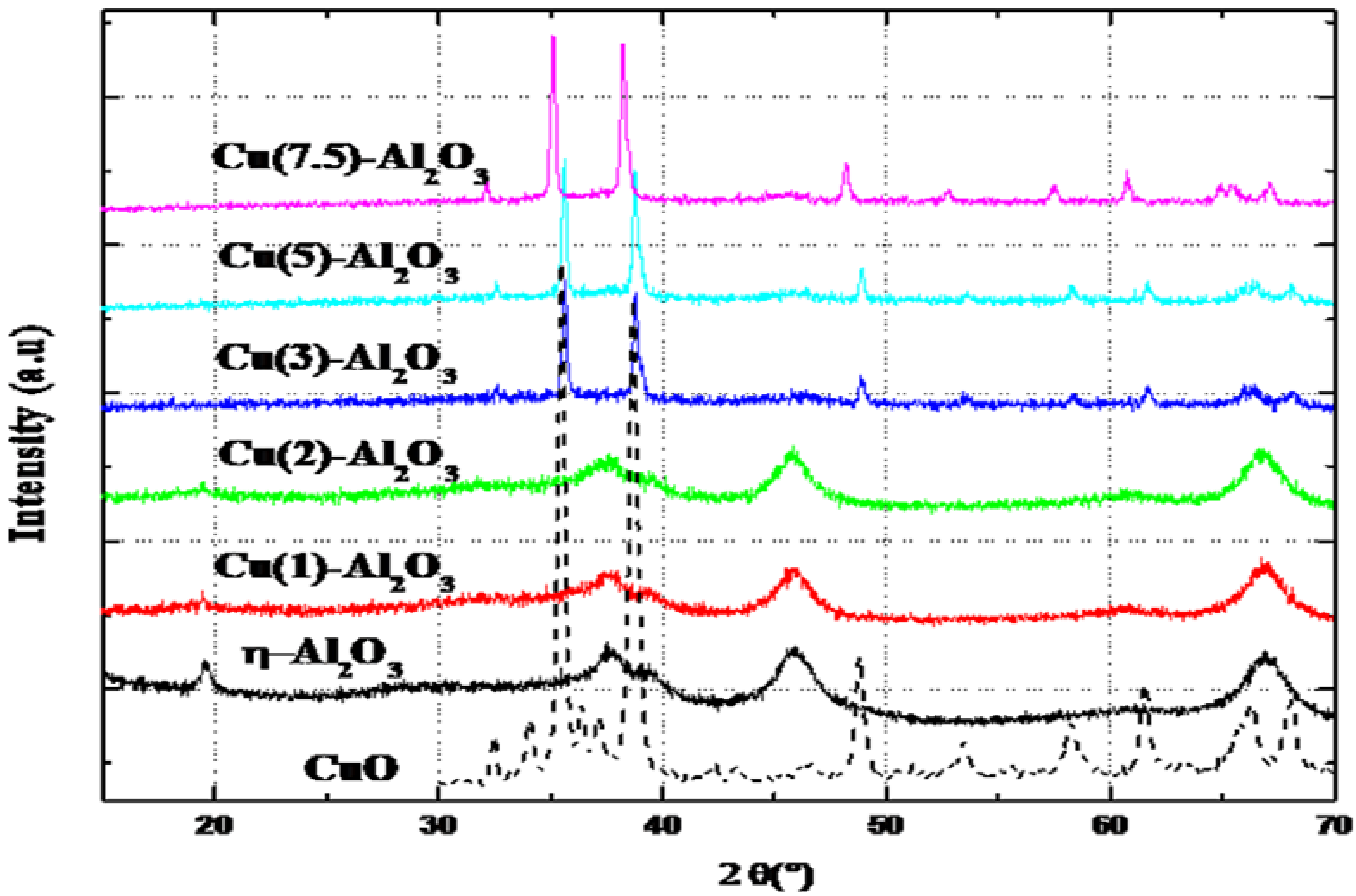


Figure 2

XRD patterns of η-Al2O3, CuO and the prepared catalysts Cu(x)-Al2O3.

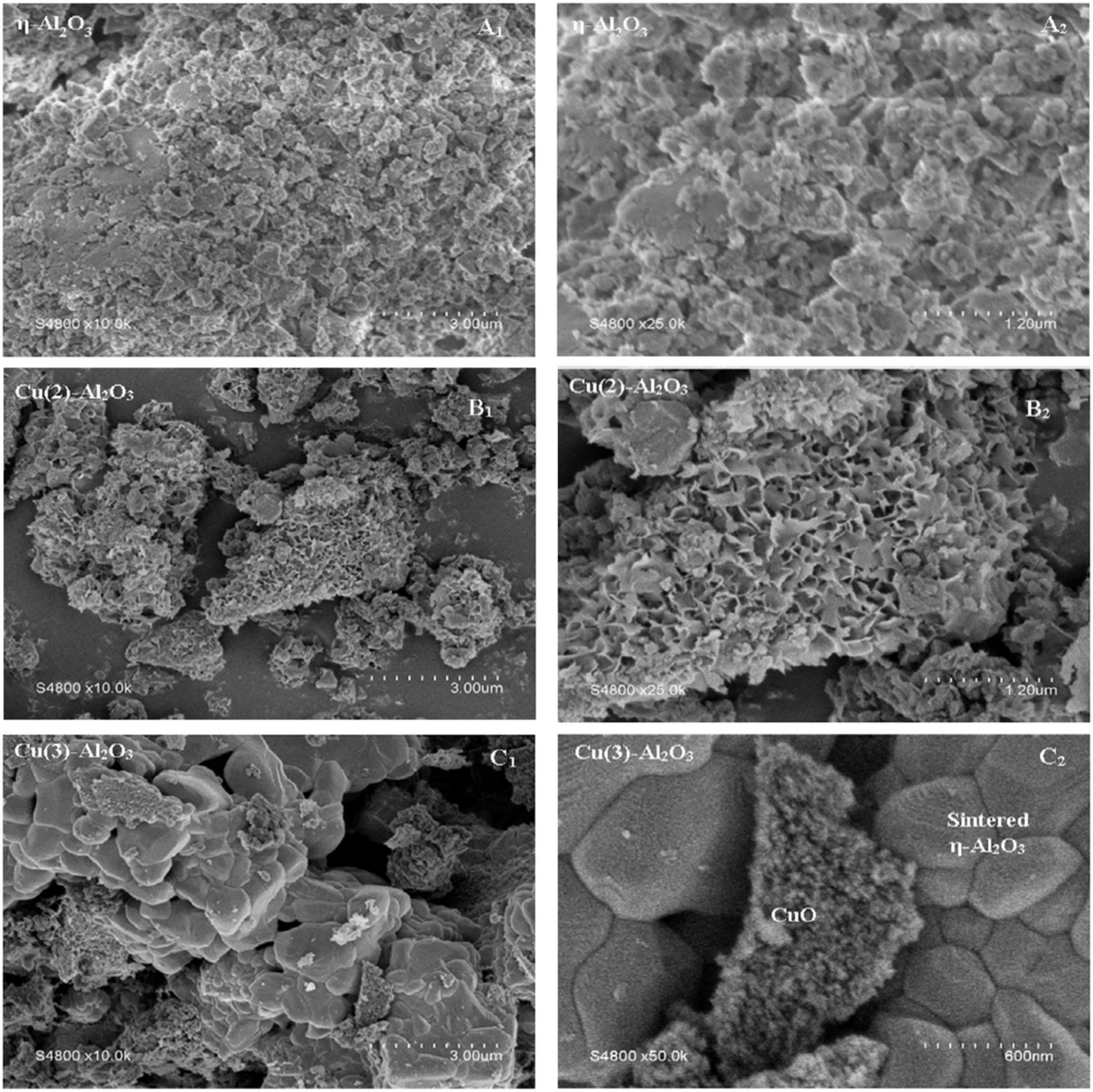


## Figure 3

SEM images of (A1, A2) the support η-Al2O3 and the catalysts (B1, B2) Cu(2)-Al2O3 (C1, C2) Cu(3)-Al2O3 with different magnifications.

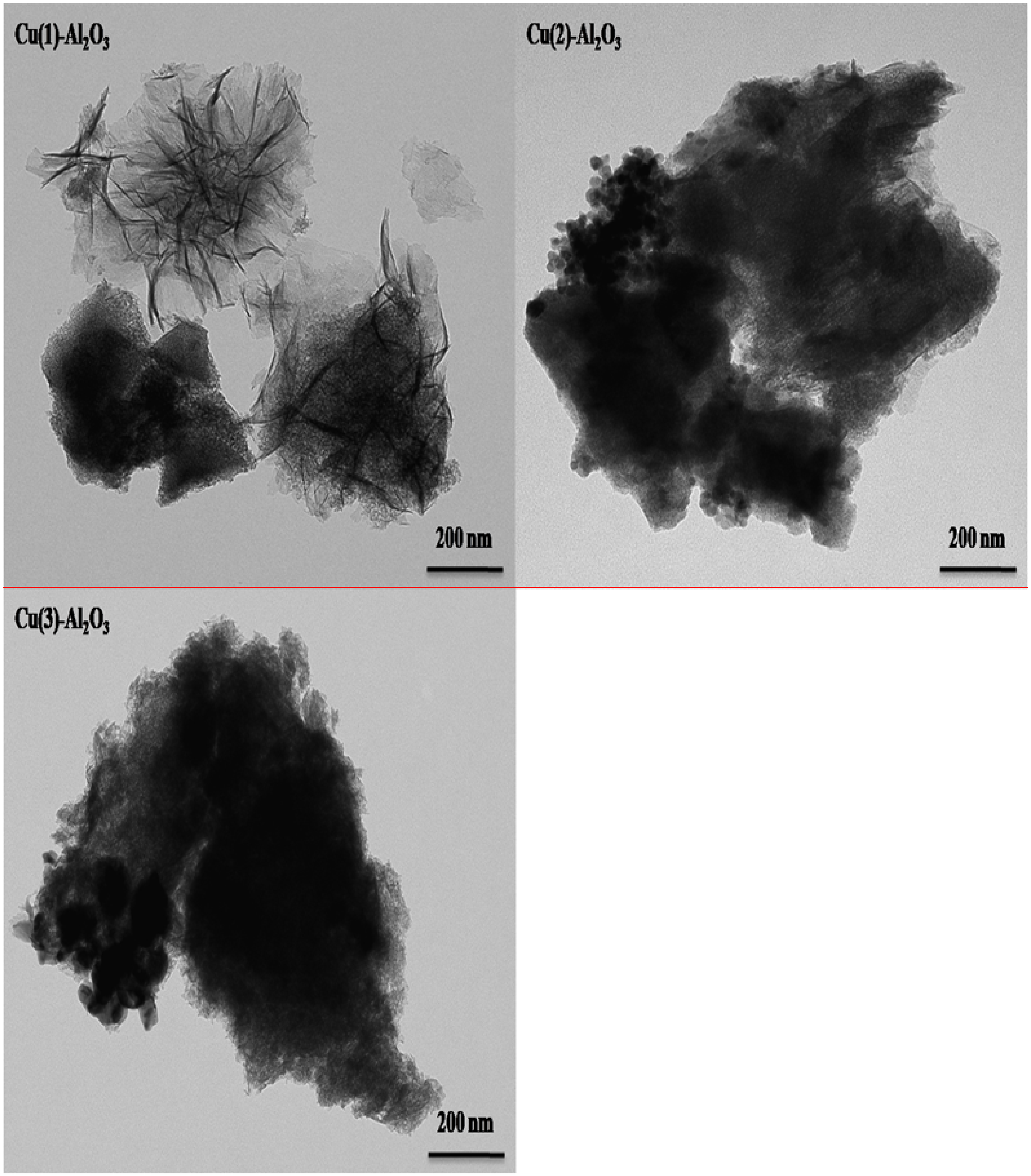


## Figure 4

TEM images of Cu(1)-Al2O3 Cu(2)-Al2O3 and Cu(3)-Al2O3 catalysts.

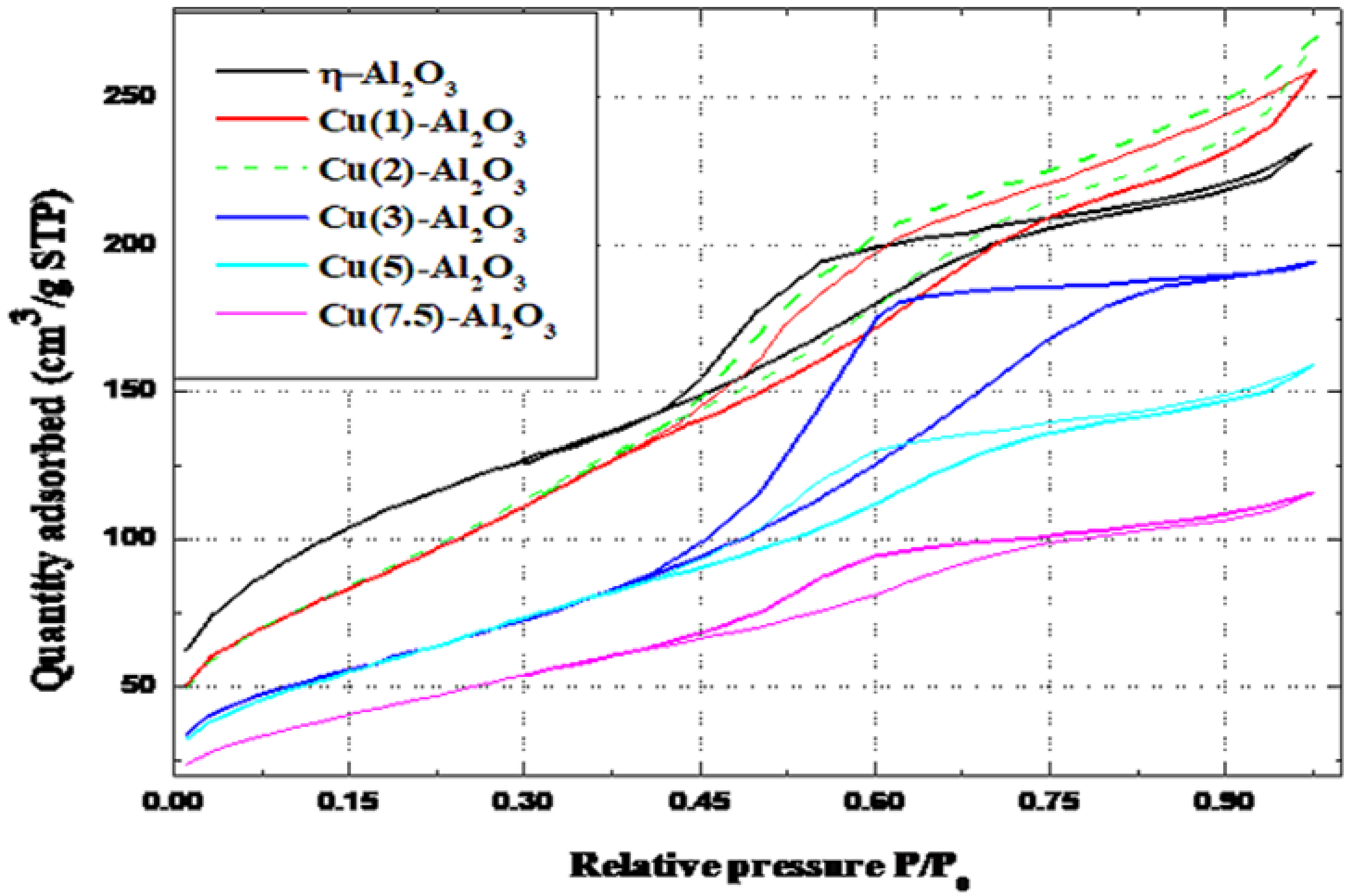


Figure 5

Adsorption−desorption isotherms of η-Al2O3 and Cu(x)-Al2O3 catalysts.

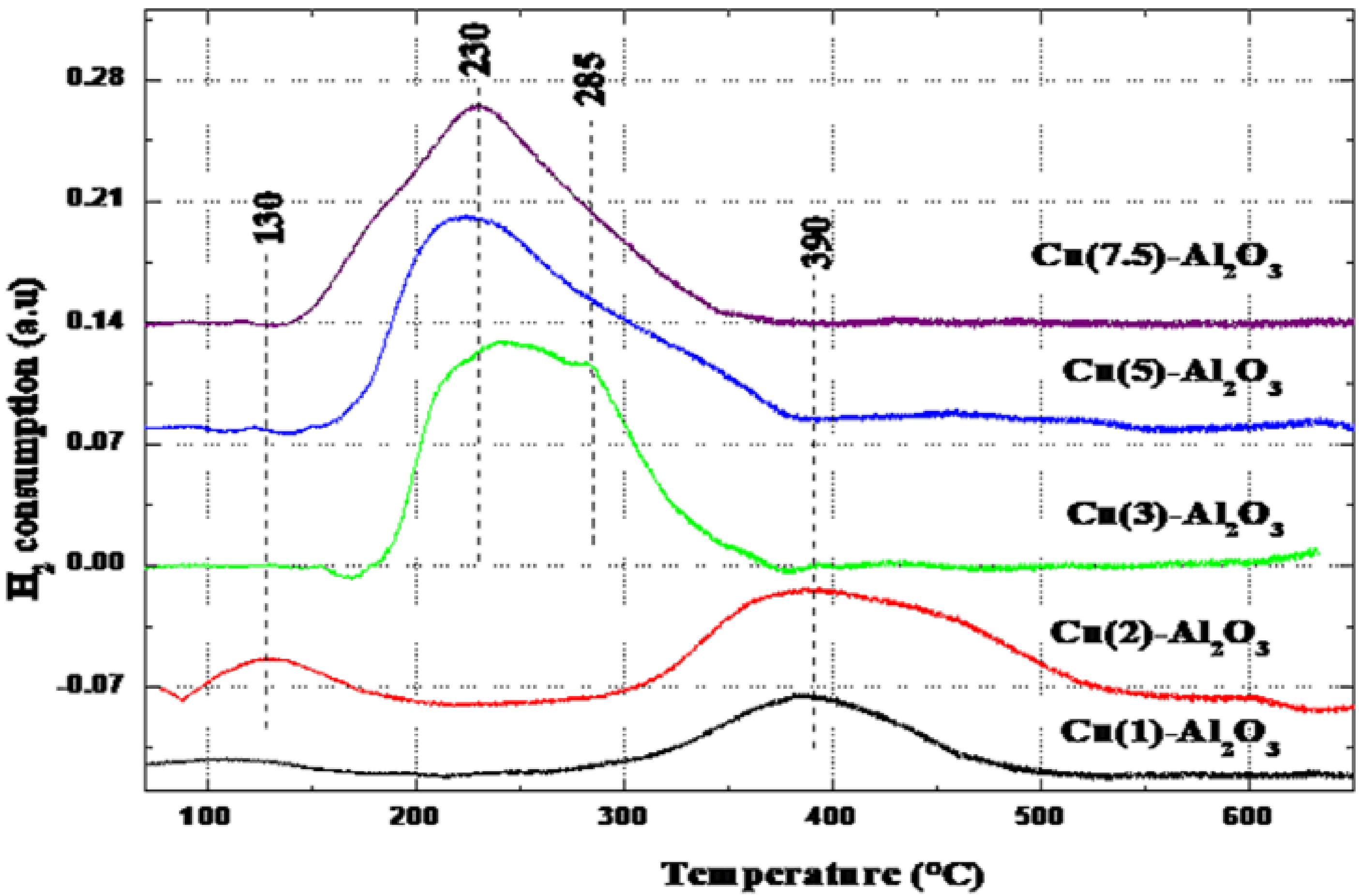


**Figure 6**

H2-TPR profiles of Cu(x)-Al2O3 catalysts.

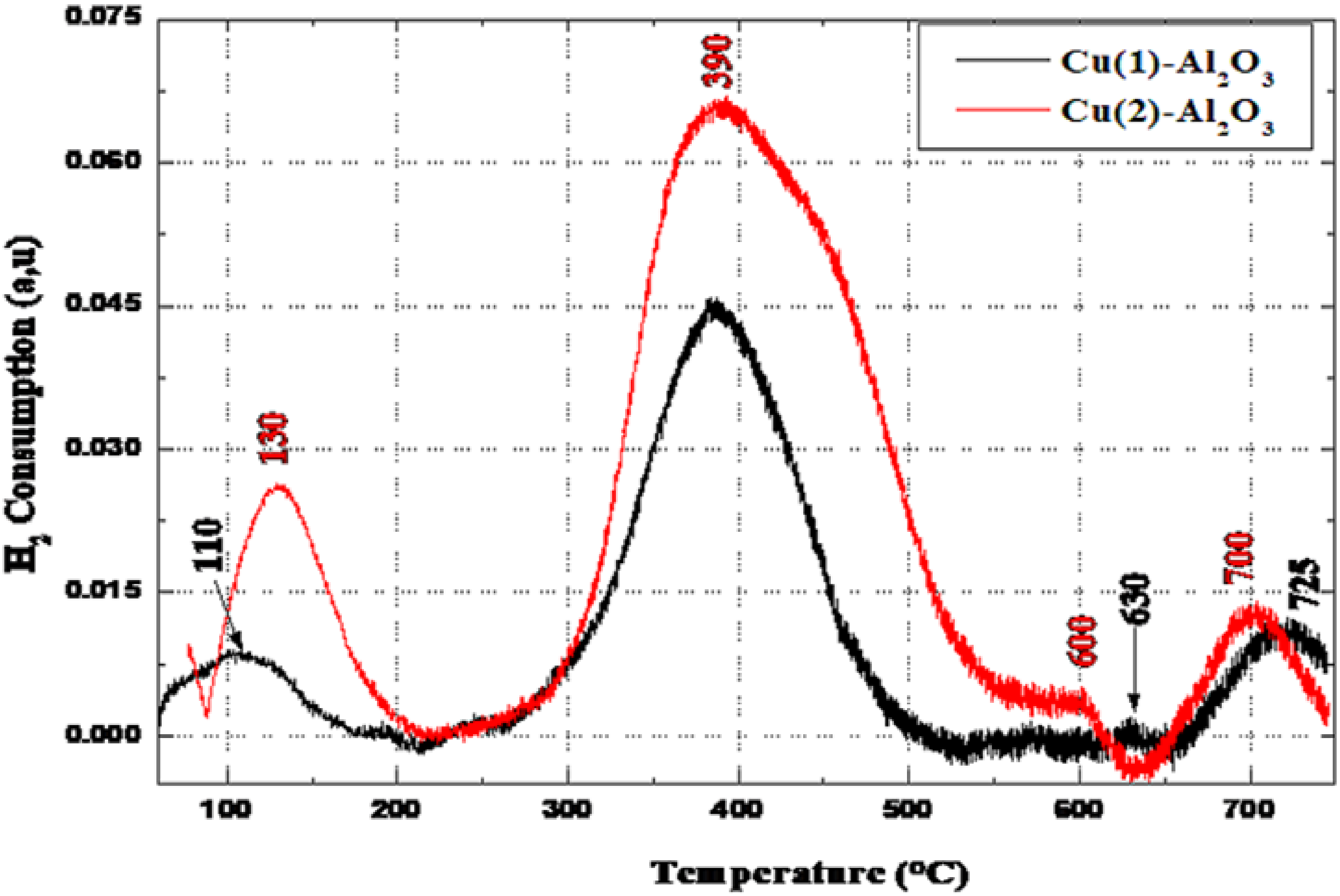


Figure 7

H2-TPR profiles of Cu(1)-Al2O3 and Cu(2)-Al2O3 catalysts.

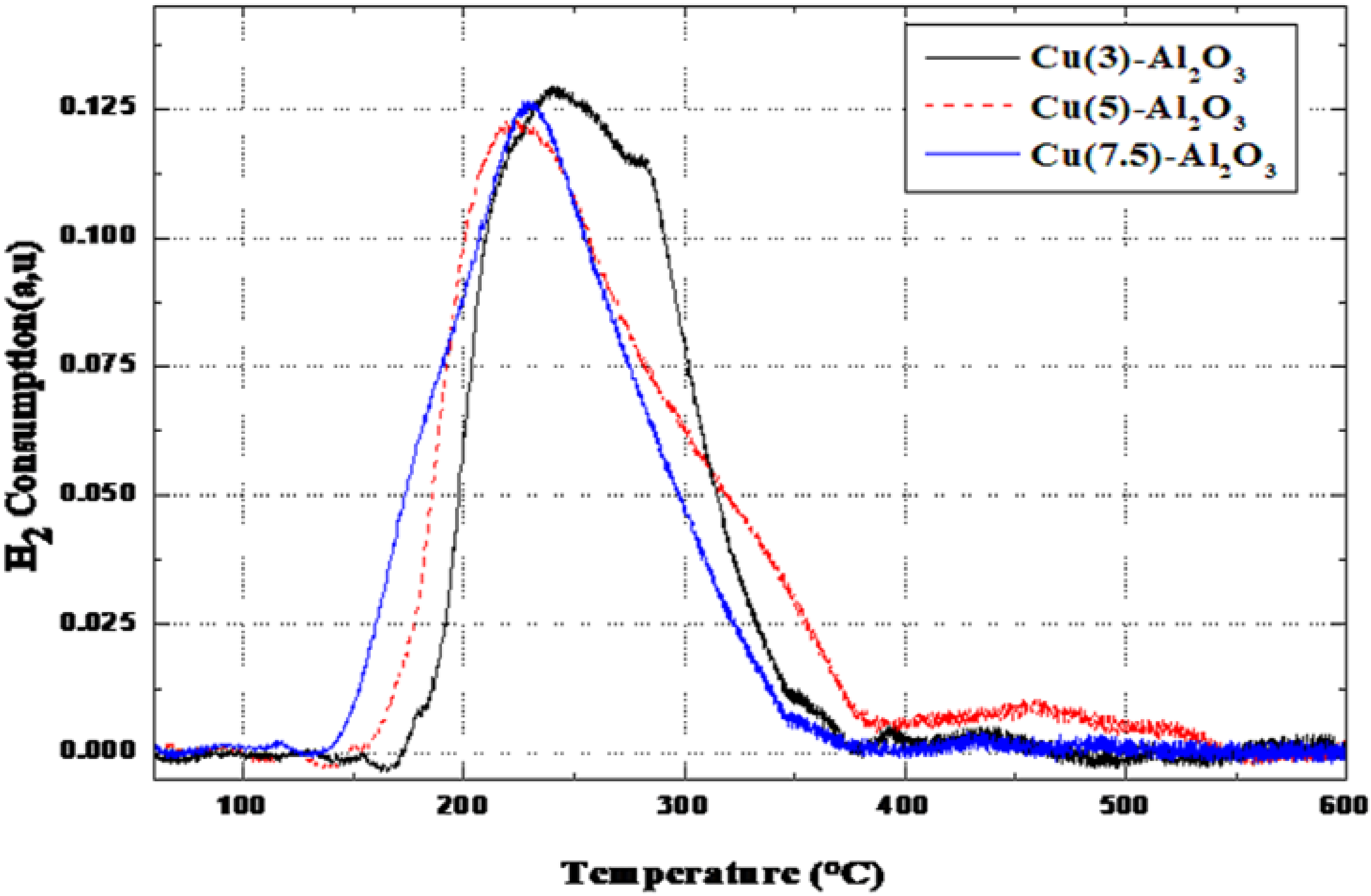


Figure 8

H2-TPR profiles of Cu(3)-Al2O3,Cu(5)-Al2O3 and Cu(7.5)-Al2O3 catalysts.

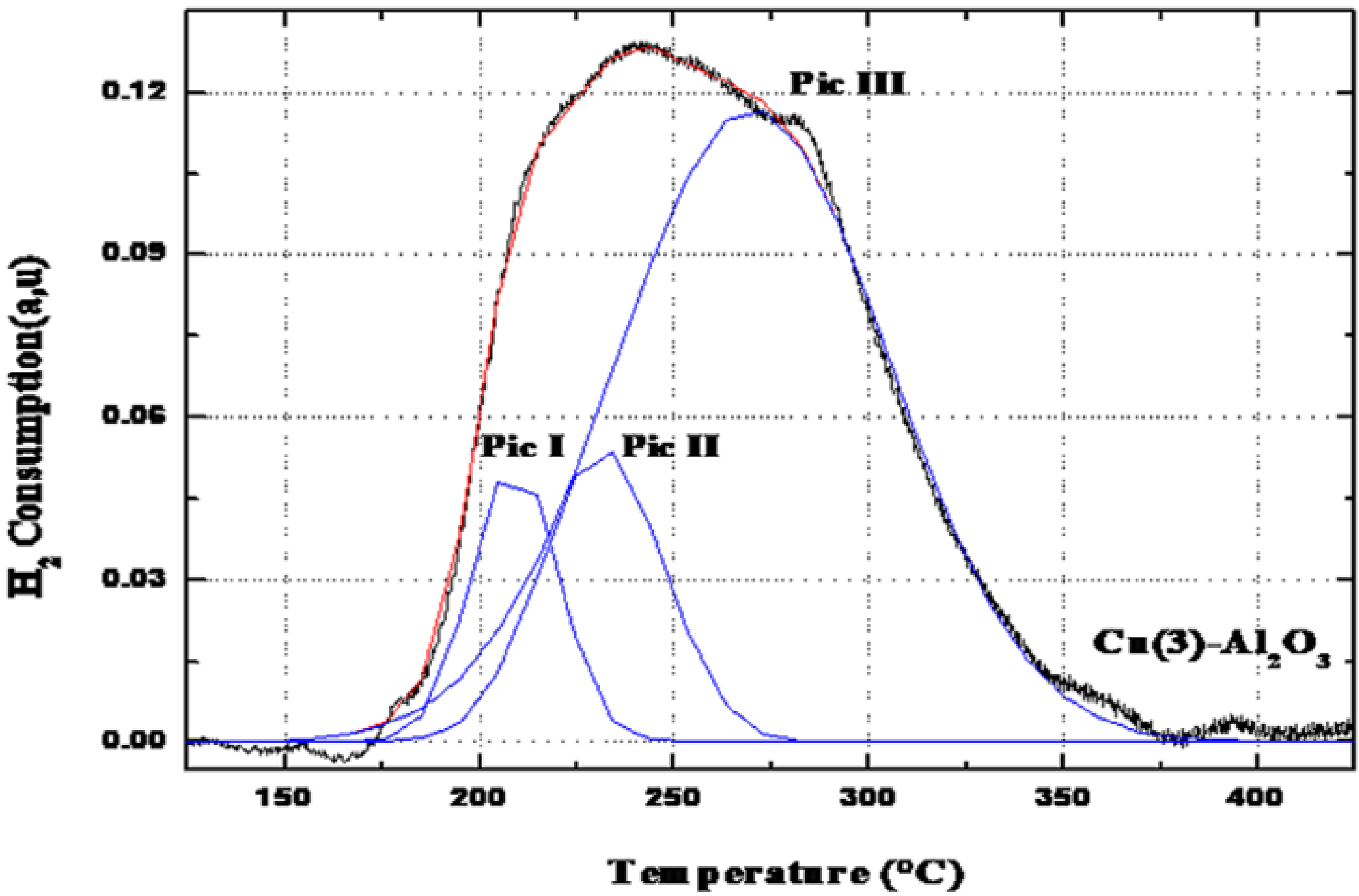


Figure 9

Deconvolution of the H2-TPR profile of the Cu(3)-Al2O3 catalyst.

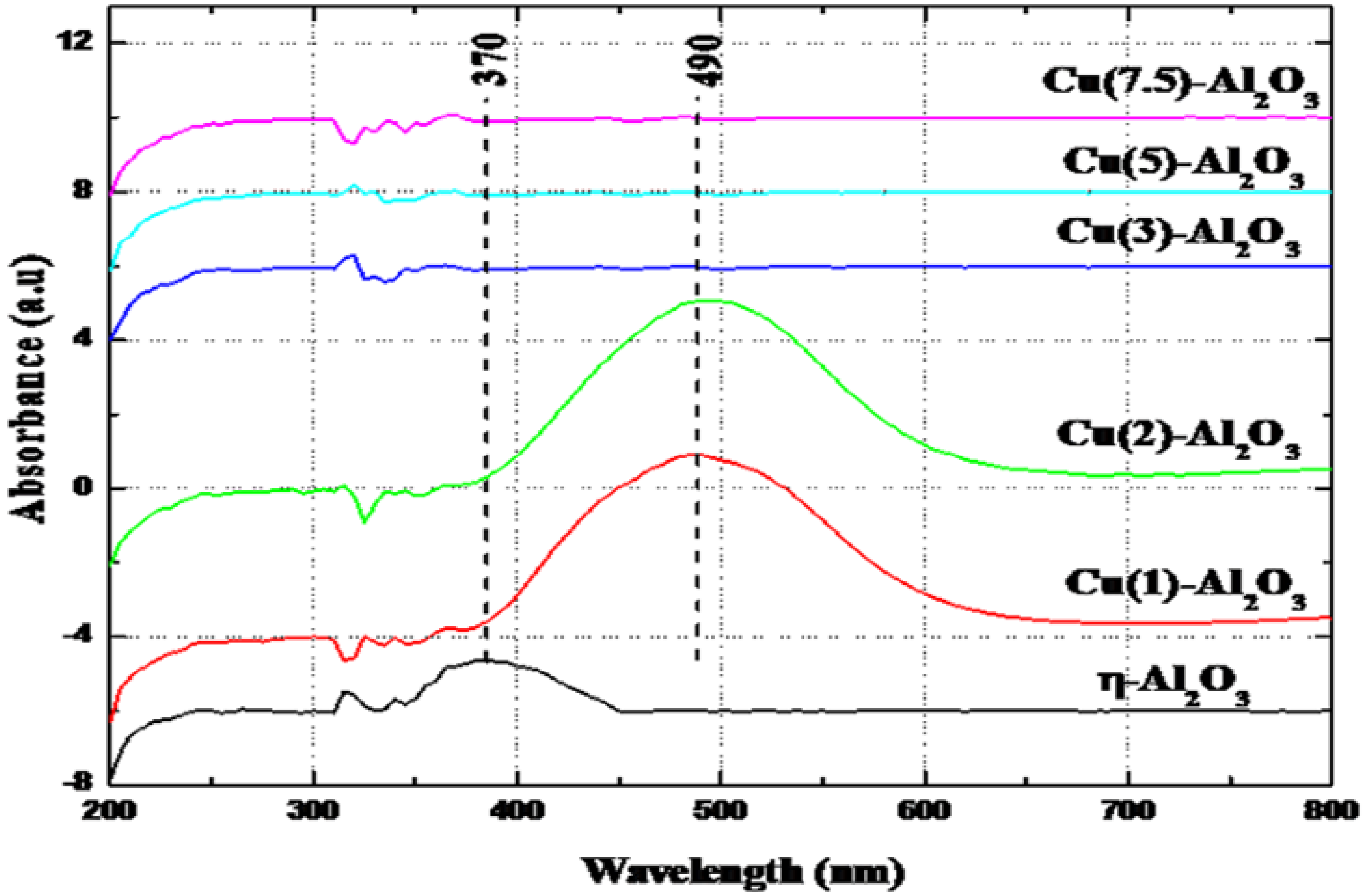


Figure 10

UV-vis spectra of η-Al2O3 and Cu(x)-Al2O3 catalysts.

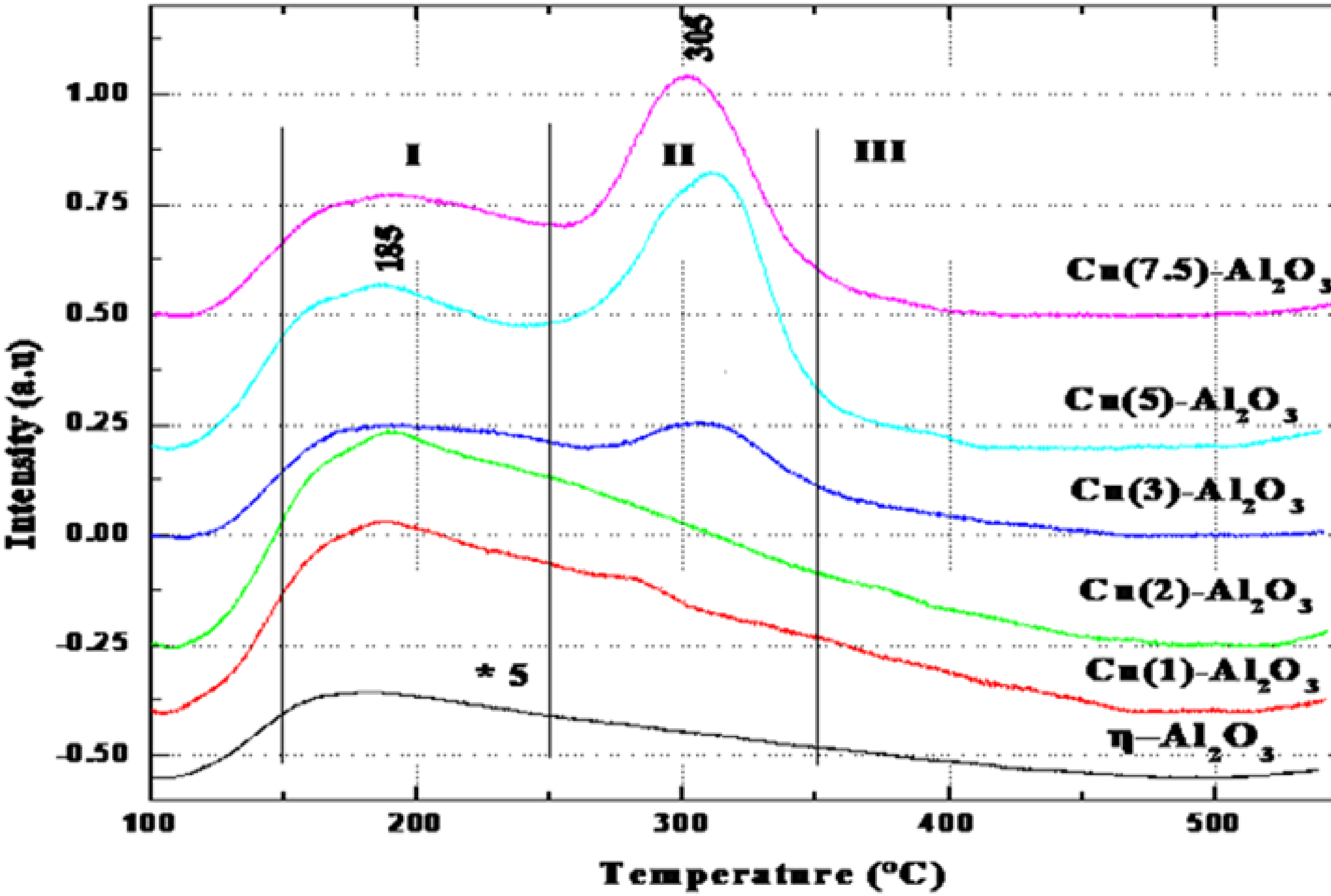


Figure 11

NH3-TPD profiles of η-Al2O3 and Cu(x)-Al2O3 catalysts.

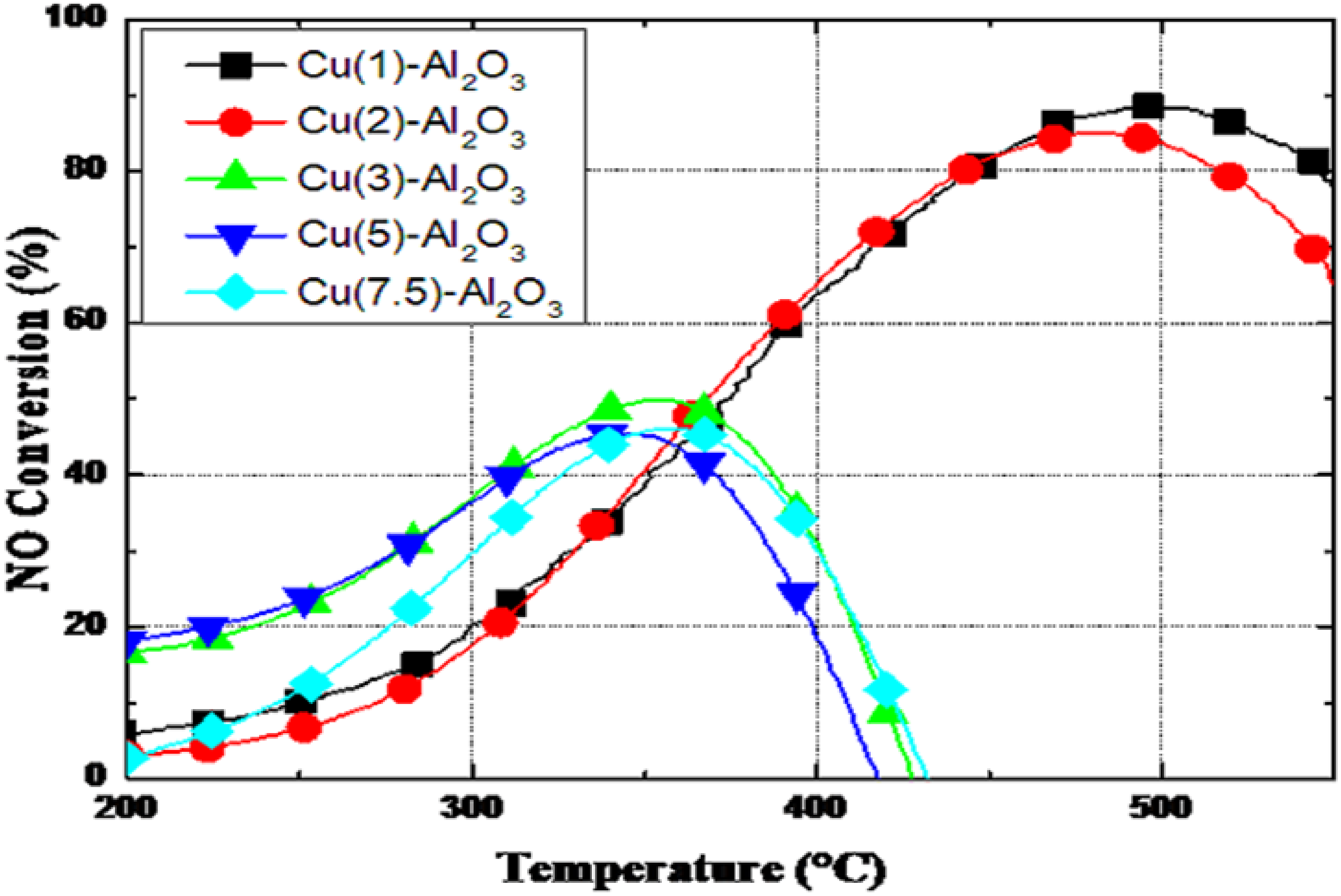


Figure 12

NO conversion profiles of the prepared Cu(x)-Al2O3 catalysts in the NH3-SCR of NO.

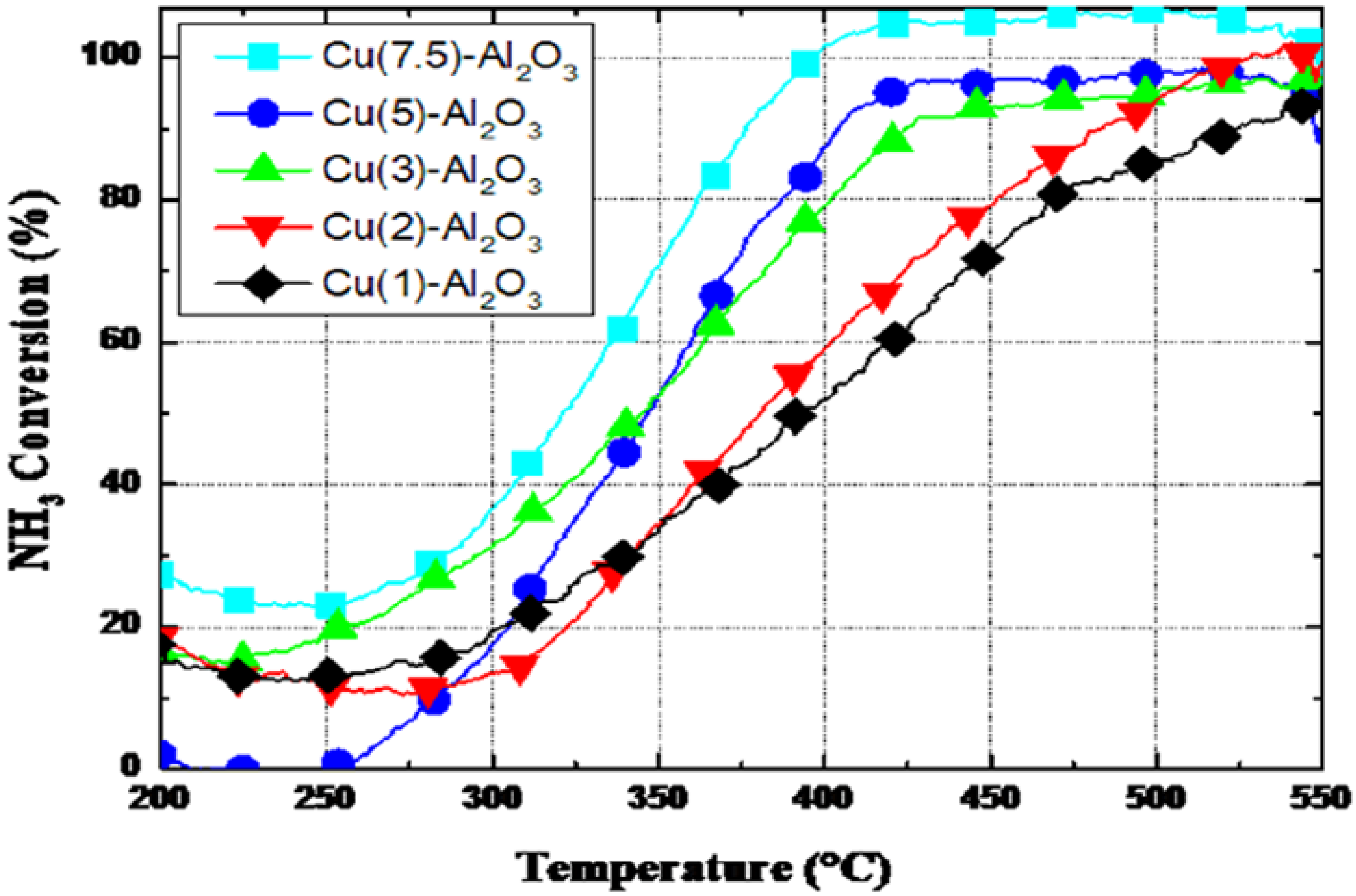


**Figure 13**

NH3 conversion profiles of the prepared Cu(x)-Al2O3 catalysts in the NH3-SCR of NO.

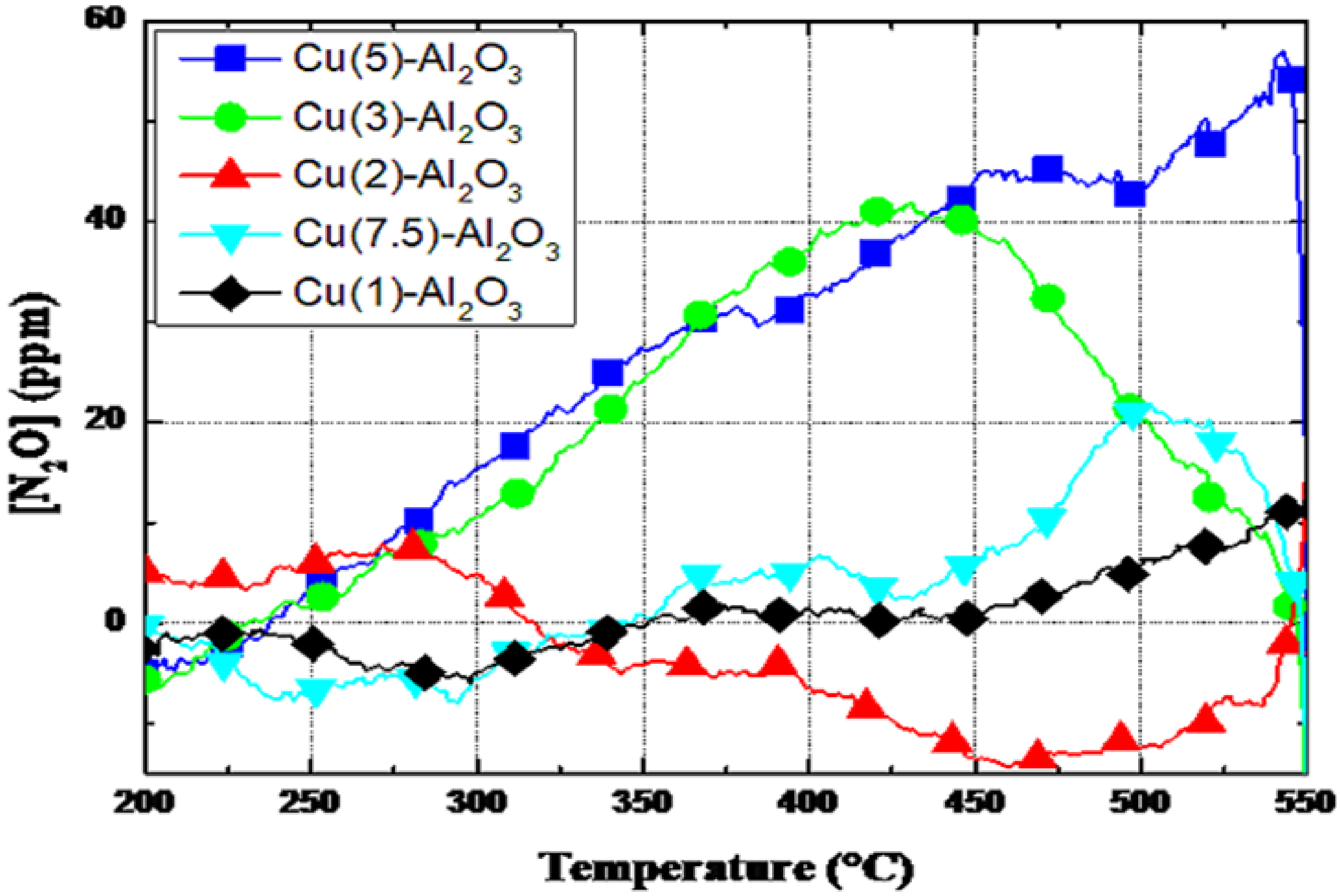


Figure 14

N2O emission profiles during the NH3-SCR of NO on Cu(x)-Al2O3catalysts.

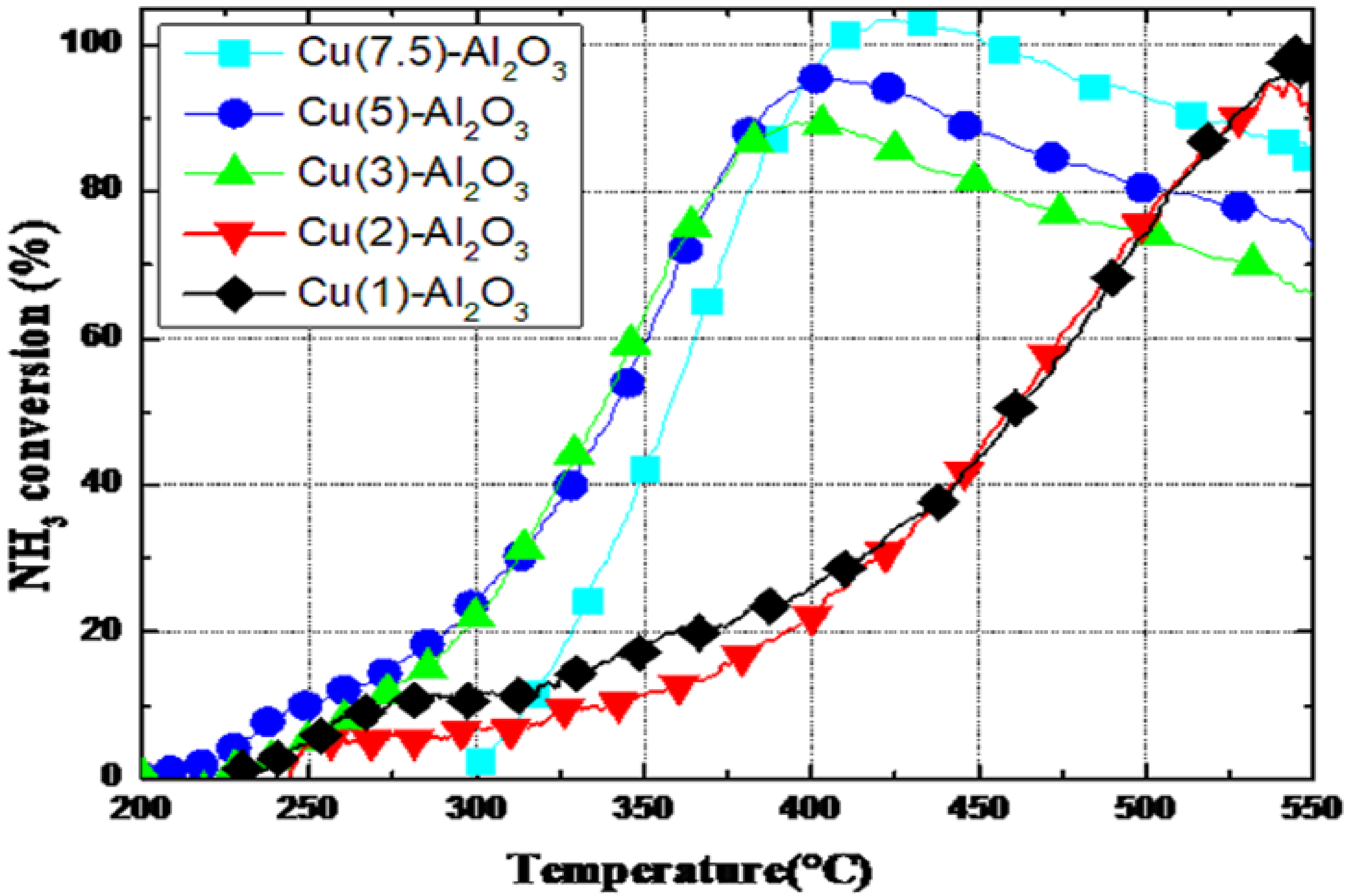


Figure 15

NH3 oxidation profiles of Cu(x)-Al2O3 catalyst

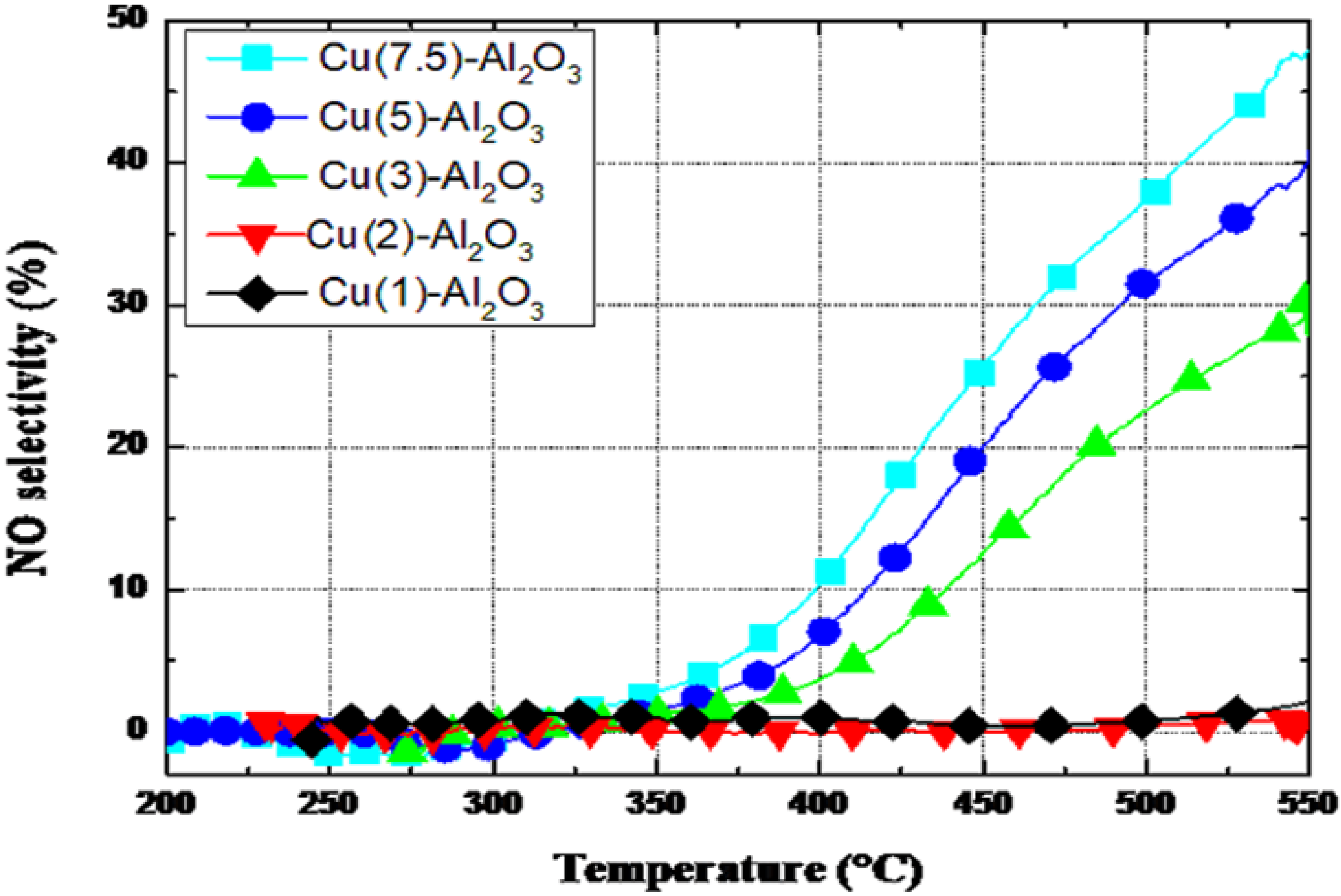


Figure 16

NO selectivity profiles obtained for NH3-SCO performed over Cu(x)-Al2O3catalysts.

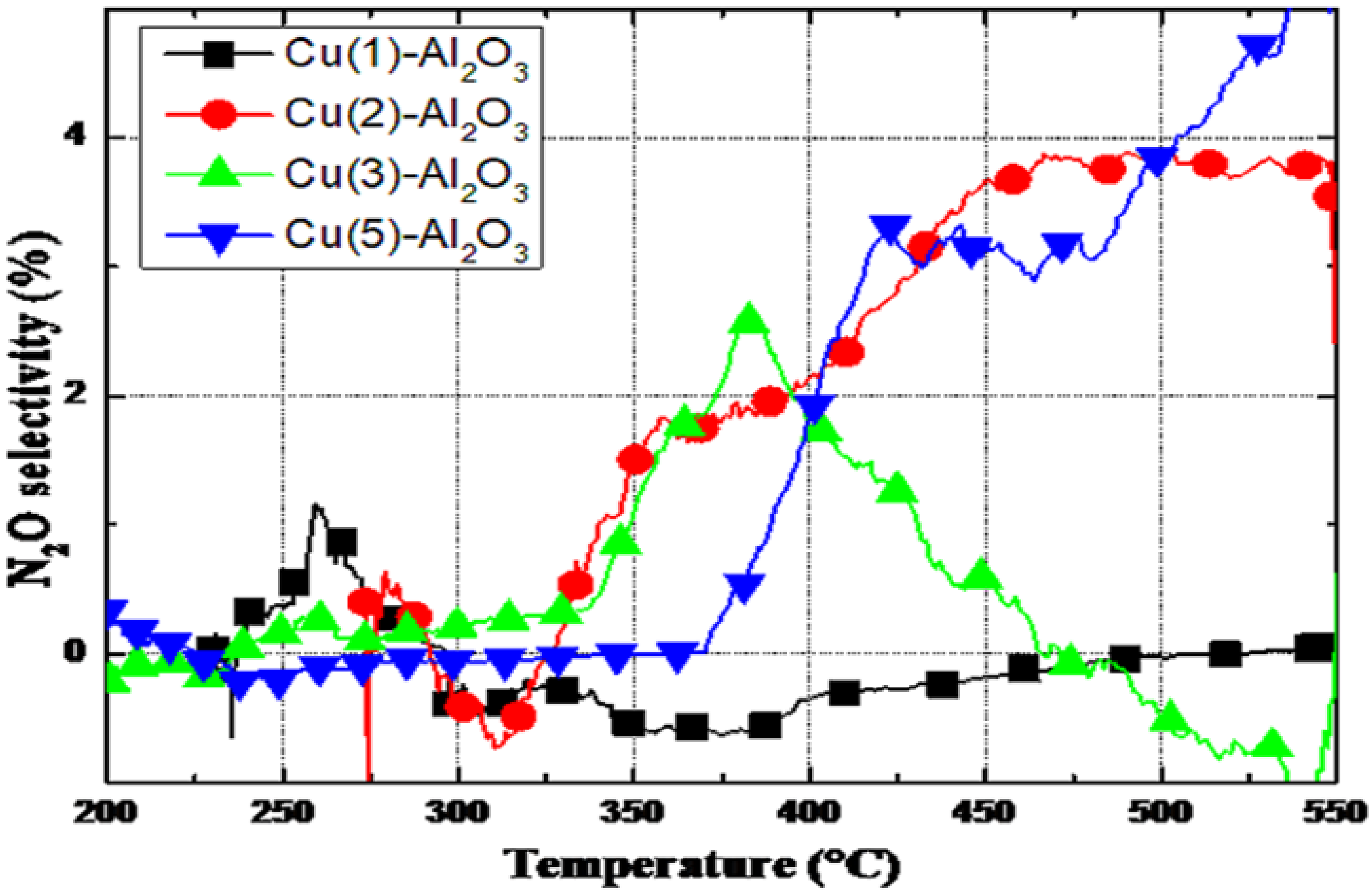


**Figure 17**

N2O selectivity profiles obtained for NH3-SCO performed over Cu(x)-Al2O3catalysts.

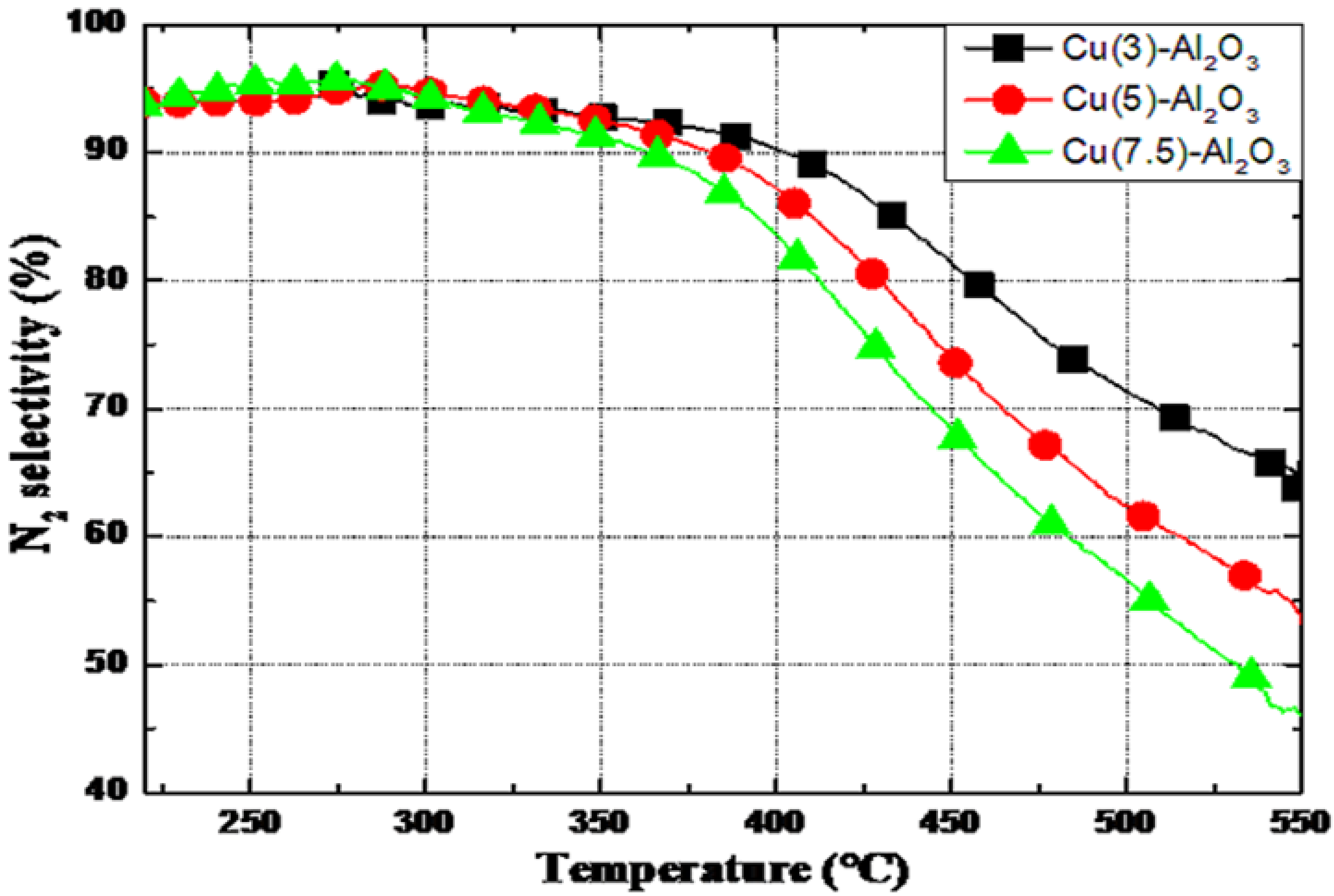


Figure 18

N2 selectivity profiles obtained for NH3-SCO performed over Cu(x)-Al2O3catalysts.